Fatigue and Damage Tolerance of Friction Stir Welds in Fibre Metal Laminates

L.D. Doppenberg

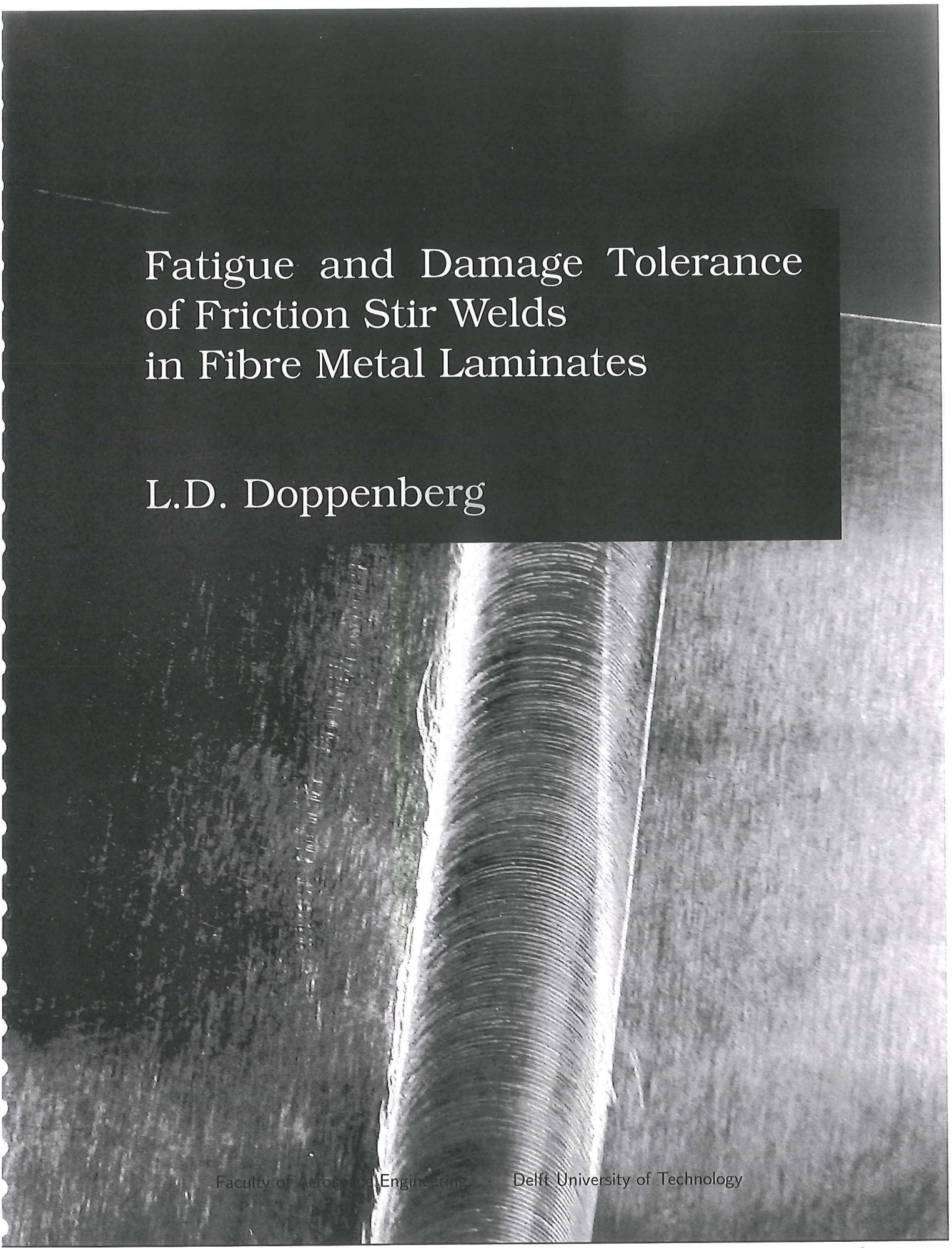

Faculty of Aerospace Engineering Delft University of Technology

TU Delft Delft University of Technology

[This page intentionally left blank]

Fatigue and Damage Tolerance of Friction Stir Welds in Fibre Metal Laminates

Master of Science Thesis

For obtaining the degree of Master of Science in Aerospace Engineering at Delft University of Technology

L.D. Doppenberg

March 30, 2015

Faculty of Aerospace Engineering · Delft University of Technology

Delft University of Technology
Faculty of Aerospace Engineering
Department of Aerospace Structures and Materials

GRADUATION COMMITTEE

Dated: March 30, 2015

Chair holder:

Dr.ir. R.C. Alderliesten

Committee members:

Dr. D.I. Gransden

Dr. C. Kassapoglou

Ir. J. Sinke

Summary

Fatigue and Damage Tolerance of Friction Stir Welds in Fibre Metal Laminates

Derk Doppenberg

Splicing is a method for joining Fibre Metal Laminate (FML) panels in which, at the location of the joint, metal sheets are overlapped to form a Damage Tolerant (DT) bond. This joining method is successfully applied in aircraft structures, but has one main disadvantage; it cannot be used in structures with significant double curvature. To qualify FMLs for these specific locations as well, a different joining method is required. With this in mind, the idea of Friction Stir Welded (FSW-ed) FMLs was born. By FSW-ing individual metal sheets together before lay-up, it is possible to create FML structures with the required double curvature. This research was aimed at developing the DT design principles for successful application of this concept in aircraft structures.

In order to reach this goal, a step-by-step DT compliance plan was created. This plan started with the identification of analytical methodologies for predicting the DT performance of the joint. In the following steps, the relations between the DT properties of FSW-ed Glare 3-3/2-0.4 and standard Glare 3-3/2-0.4 were determined experimentally, and used to design different concepts that met the requirements from the compliance plan. Out of the four concepts, the idea with the highest value in terms of cost-effectiveness was determined, which was subsequently compared to other materials typically used in the aerospace industry.

Experimental results show that cracks grow faster in- and residual strength is lower of- the FSW-ed version of the laminate. To bring the DT performance back to the level of the standard laminate, additional layers of material are necessary at the location of the joint. The concept that does this in the most cost-effective way for Glare 3-3/2-0.4, is a joint with an inter-laminar aluminum doubler of the same thickness as the other metal layers. Compared to the spliced version of the laminate, the FSW-concept is significantly more expensive. When looking at the DT performance compared to other materials, only certain carbon-fibre reinforced plastics have better properties.

Acknowledgements

Although the front page of this thesis suggests that all of the work was done by one person, none of it would have been possible without the help of others. I take this opportunity to acknowledge some of the people who contributed to the final results of this thesis.

First of all, I would like to thank my supervisor, René Alderliesten, for his support and guidance during the research period. His effort to monitor the technical contents and writing process have significantly improved the quality of the work.

I am also very grateful to the technicians of the Aerospace Structures and Materials Laboratory for their assistance during the experimental part of the project. These people spent a lot of time helping with the manufacturing of the test pieces and setting up the testing machines and measuring devices.

Not directly related to the technical contents of this research, are the people who showed up on the local football pitch every Friday afternoon. These people did not provide me with the answers to any of my research questions, but did shift the focus to football and therefore provided the necessary fun and relaxation during the working week.

Finally, I would like to thank my family for their continued support throughout this adventure. Their interest and enthusiasm kept me motivated to finish the work. Without them none of this would have been possible. Special thanks to my parents, who have provided me with the attitude and means to finish my studies.

Contents

List of Tables

List of Figures

List of Symbols

Symbol	Units	Description
A	mm^2	Area
a	mm	Half crack length
a_0	mm	Initial half crack length
a_{eff}	mm	Effective crack length
a_{phys}	mm	Physical crack length
C_{cg}	$\frac{m}{MPa\sqrt{m}}$	Paris law constant
C_{man}	€	Manufacturing costs
C_P	–	Crack growth retardation parameter
DR_{eff}	–	Effective damage ratio
DR_{FSW}	–	Damage ratio FSW-ed layer
E_x	MPa	Young's modulus in x-direction
E_y	MPa	Young's modulus in y-direction
f	Hz	Frequency
f_0	–	Geometrical correction factor
f_{br}	–	Nondimensional bridging stress intensity factor
f_e	–	Emission function
f_n	–	Noise function
f_{lcc}	–	Life-cycle cost function
G_{xy}	MPa	Shear Modulus
K	$MPa\sqrt{m}$	Stress intensity factor
$K_{farfield}$	$MPa\sqrt{m}$	Far-field stress intensity factor
K_G	$MPa\sqrt{m}$	Energy release rate intensity unit
$K_{opeining}$	$MPa\sqrt{m}$	Crack opening stress intensity factor
K_R	$MPa\sqrt{m}$	Crack resistance intensity unit
K_{tip}	$MPa\sqrt{m}$	Stress intensity factor at crack tip
M	–	Rotation matrix
M_s	kg	Mass of structure
MVF	–	Metal volume fraction
m	–	Weight factor
m_0	–	Weight function
m_{br}	–	Bridging weight function
N	–	Number of load cycles
N_{fail}	–	Number of cycles till failure
n_{cg}	–	Paris law constant
p	$€/kg$	Life-time fuel cost factor
R	–	Stress ratio
S_{lam}	MPa	Stiffness matrix laminate
S_R	MPa	Residual strength
S_ϕ	MPa	Rotated stiffness matrix
s	mm	Distance between starter notches

T	K	Temperature
t_{al}	mm	Thickness aluminum layer
t_{lam}	mm	Thickness laminate
t_p	mm	Thickness layer p
V_{al}	$-$	Volume fraction aluminum
V_{FSW}	$-$	Volume fraction welded material
V_{pre}	$-$	Volume fraction prepreg
W	mm	Width of panel
WVF	$-$	Weld volume fraction
α_{lam}	K^{-1}	Coefficient of thermal expansion laminate
β_f	$-$	Nondimensional fibre-bridging factor
ΔK_{eff}	$MPa\sqrt{m}$	Effective stress intensity factor range
ΔT	K	Difference in curing and operating temperature
μ_{xy}	$-$	Poisson's ratio xy-direction
μ_{yx}	$-$	Poisson's ratio yx-direction
σ	MPa	Stress
σ_0	MPa	Stress on crack face
σ^b	Mpa	Bending stress
σ_c	MPa	Critical stress level
σ_{lam}	MPa	Stress applied on laminate
σ_{pre}	MPa	Precrack stress
σ_{res}	MPa	Residual stress
σ_u	MPa	Ultimate strength
σ_y	MPa	Yield strength
σ_ϕ	MPa	Stress matrix layer p

Acronyms

AD	Artificial Damage
AS	Advancing Side
CA	Constant Amplitude
CGL	Crack Growth Life
CFRP	Carbon Fibre Reinforced Plastic
CLT	Classical Lamination Theory
COD	Crack-Opening Displacement
DOC	Direct operating cost
DSG	Design Service Goal
DR	Damage Ratio
DT	Damage Tolerance
GFRP	Glass Fibre Reinforced Plastic
HAZ	Heat-Affected Zone
ISP	Inspection Starting Point
FML	Fibre Metal Laminate
FSW	Friction Stir Weld
LOV	Limit Of Validity
MSD	Multiple Site Damage
MVF	Metal Volume Fraction
RS	Retreating Side
SIF	Stress Intensity Factor
SMP	Structural Modification Point
SSD	Single Site Damage
TMAZ	Thermo-Mechanically Affected Zone
VA	Variable Amplitude
WFD	Widespread Fatigue Damage
WVF	Weld Volume Fraction

1 Introduction

Tim Clark, president of Emirates Airline, once said that the Airbus A380 "defies gravity" from a business point of view. By using the latest advances in flight control systems, propulsion technology and materials the A380 has become one of the most prestigious aircraft in the world [1, 2]. Part of this success story can be ascribed to the material Glare. Glare is a hybrid material consisting of alternate layers of aluminum alloy and glass fibre reinforced adhesive. Due to its excellent fatigue- and damage tolerance characteristics compared to standard aluminum alloys [3] the material offers a significant reduction in weight.

In the current generation of aircraft Glare is mainly used in the upper and lateral parts of the fuselage. For an aircraft as big as the A380 this means that large sheets of aluminum are required. Although it is possible to produce aluminum sheets of the desired thickness at the required length, producing them at the required width proves to be difficult [4]. In order to overcome this problem the aluminum sheets in the Glare panels are overlapped in the longitudinal direction of the fuselage. The joining method applied here is called the 'splice' concept [5, 6]. By splicing the aluminum sheets it is possible to achieve the required width for application of Glare (or other Fibre Metal Laminates (FMLs)) in fuselage panels.

As can be seen from figure 1.1, Glare is predominantly used in the single-curved parts of the fuselage. Although it would be beneficial in terms of fatigue- and damage tolerance if Glare is also applied at certain locations where significant double-curvatures are required, it is not possible at the moment due to the complexity of the splice joint. One can imagine that producing joints with overlapping sheets for panels with small radius double-curvatures is difficult and interference of the joints cannot be avoided. Only if both radii are relatively large, it is possible to apply the current method at these specific locations. By simplifying the joint it should be possible to qualify the material for strongly double-curved parts as well, and maybe increase the cost-effectiveness at the same time.

A solution that meets these requirements would be to weld the aluminum sheets together before lay-up. By welding the sheets first, it is possible to introduce double-curvatures in the material. After the sheets are welded together and brought into the right shape, the laminate can be layed-up and cured. The best welding technique to use in this case is friction stir welding. Friction stir welding is, unlike many other welding techniques, suitable for welding high-strength aerospace aluminum alloys [7]. If this technique proves to be suitable as a replacement for, or addition to, the splice concept currently in use it will be possible to use Glare at locations where strong double-curvatures are required.

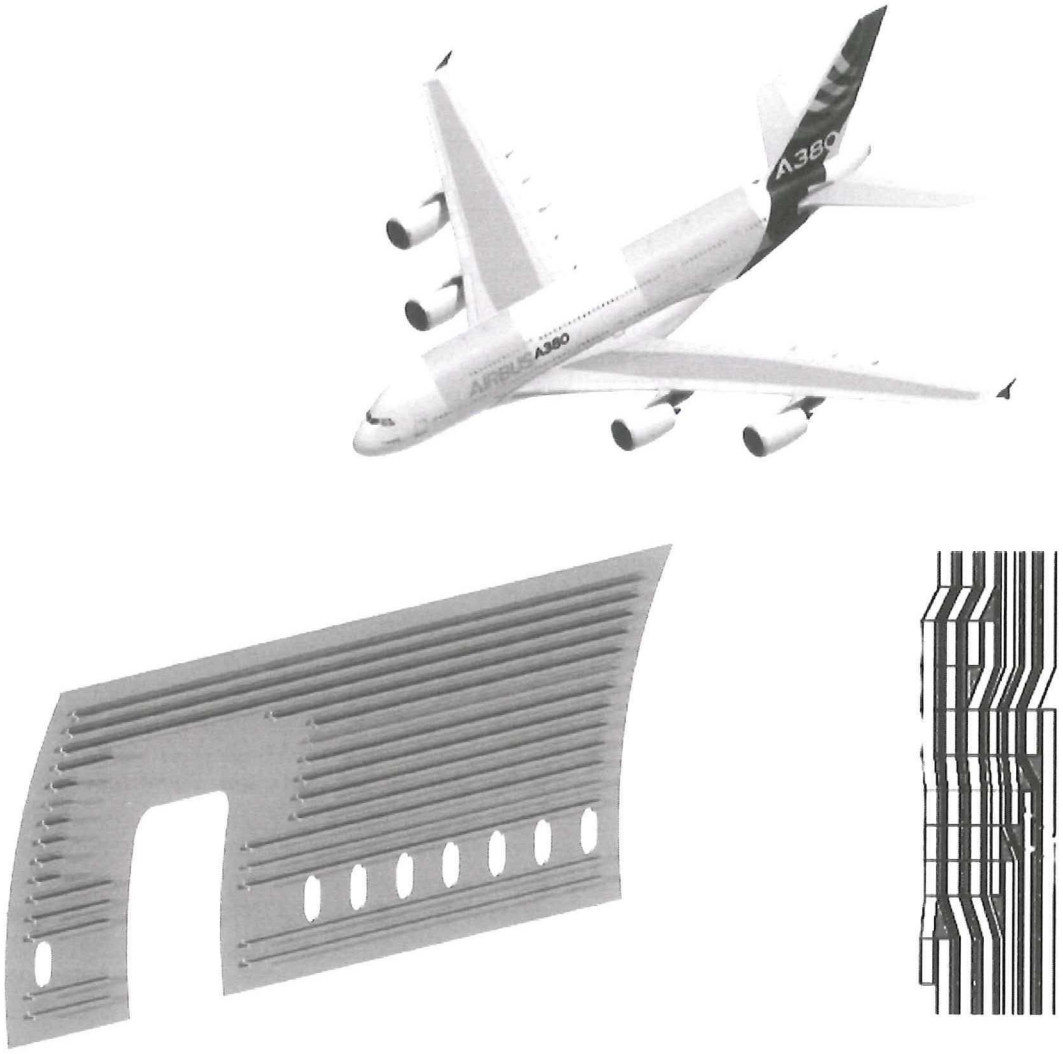

Figure 1.1: Location and configuration of splices in the Airbus A380 [2, 8].

Before this technique can be applied in aircraft structures it is necessary to design the new joints and certify the concepts. One of the areas that requires special attention in this process is the performance in terms of fatigue- and damage tolerance. Bied-Charreton [9] investigated the possible damage situations that can occur in Friction Stir Welds (FSWs) and determined the fatigue performance of FSW-ed Glare compared to standard Glare. The current research is aimed at expanding this knowledge by including the Damage Tolerance (DT) performance and has as objective: *To make recommendations to Airbus on DT certification of FSW-ed joints in FML structures by identifying the required DT evaluation methods and establishing design guidelines for these types of joints.*

In order to reach this goal, multiple steps had to be taken. The first step was to create an overview of the knowledge available at the start of the research. This is the subject of chapter 2 in

which the main findings of the literature review are presented. Following this step is the creation of a step-by-step DT certification guide. This guide will be presented in chapter 3 and will serve as the foundation for the rest of the research. One of the things that follows directly from this guide are the requirements for the evaluation methodology. Based on these requirements, the DT evaluation methodologies will be discussed in chapter 4. To support the developed methodologies and determine the necessary material properties an experimental program has to be carried out. All of the details on the set-up and the results will be presented in chapter 5. By using the experimental results and the DT evaluation methodology, design concepts for FSW-ed FMLs were developed in chapter 6. Finally, the report will be concluded with chapter 7, in which the conclusions of this research and recommendations for further research are presented.

2

Literature Review

Having a full understanding of all the knowledge that was available in the field of interest at the start of the research was essential for the rest of the project. This information not only defined the research project, but also served as a valuable resource for methods and data at a later stage. The current chapter summarizes this knowledge and introduces the reader to the most important terms. Since all of the research revolved around the concept of FMLs, the first section in this literature review is used as a short introduction to the material. This introduction into the field is necessary to understand what FSW-ed FMLs actually are. Together with other methods for joining FMLs, this concept will be discussed in the second section. Finally, the chapter is completed by the state-of-art in DT of FSWs.

2.1 Fibre Metal Laminates

FMLs have found their way in aircraft since the eighties. It all started with the application of Arall (Aramid Reinforced Aluminum) parts on the Fokker 50. This was the first FML to be flown on a commercial aircraft. As time continued a new type of laminate was developed. This laminate, called Glare (Glass Laminate Aluminum Reinforced Epoxy), performed superiorly to Arall, and therefore became the most important FML for aerospace applications [4].

A FML is best described as a laminate of multiple thin metal layers bonded by layers of composite material. The general concept is illustrated in figure 2.1, in which the different layers are clearly visible.

Glare, for example, is built up from thin aluminum alloy 2024-T3 sheets and prepreg layers consisting of S2-glass fibres in FM94 adhesive. By varying the number of aluminum layers, the thickness of the aluminum sheets, number of prepreg layers in between the aluminum sheets, and the orientation of the prepreg layers, different grades of Glare can be manufactured. These grades have different mechanical properties and can therefore be used for different purposes.

2.2 Joining methods FMLs

Just like there are different sorts of FMLs, also different methods for joining them exist. One of these methods (splicing) was already introduced. This method is based on overlapping the aluminum sheets and filling the resulting hollow spaces with epoxy.

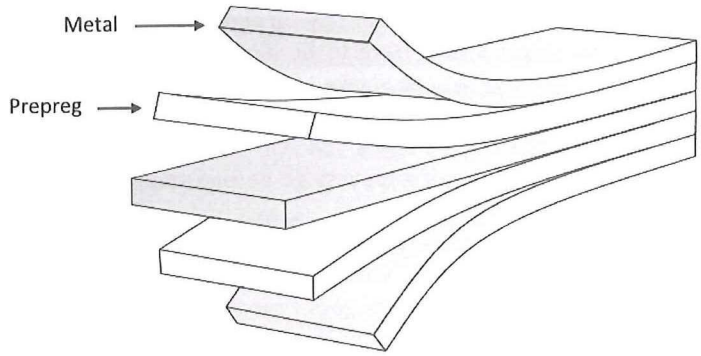

Figure 2.1: Example of a Fibre Metal Laminate, showing the metal and prepreg layers [10].

Whereas this is a method solely applicable to FMLs and composites, a solution that is also used with other materials is to mechanically fasten the different panels. An example of this joining method applied to FMLs is shown in figure 2.2a (note that the figure only shows the general concept and does not necessarily display an actual application). Mechanical fastening involves the use of rivets or bolts to join the panels. These panels can either be joined directly (lap-joint), or by using an extra metal or FML strip (but-joint).

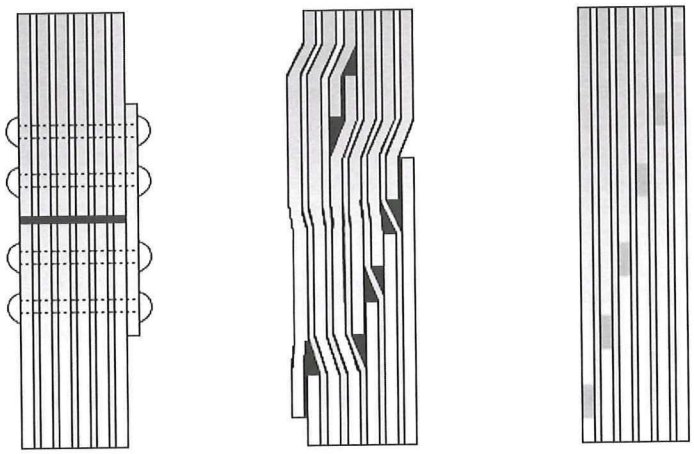

(a) Mechanical (b) Splicing (c) FSW

Figure 2.2: Three different methods for joining FML panels. (Note: not to scale, Image edited from [8])

Compared to mechanical joints splices are more durable, since they are less sensitive to moisture ingress and delamination. Although splices have proven to be a viable solution to joining FML sheets, improvements are still possible. As can be seen from figure 2.2b, the splice is a relatively complex joint. Joints like this are difficult to manufacture and provide problems when used at locations where double curvatures are required. Both of these problems can be overcome by using the FSW-ed FML,

shown in figure 2.2c. The design of this joint is relatively simple compared to the splice; individual metal sheets are welded together, after which the lay-up and curing can occur. One of the implications of this new method is that larger sheets have to be handled during lay-up. Instead of the smaller individual sheets with splicing, large welded sheets can be placed in the mold. A reduced lay-up time and minor weight savings therefore are, next to the solution to the double curvature problem, possible advantages of this joint compared to the splice concept [11].

The implications for the manufacturing process go beyond the lay-up stage. A decision has to be made at which stage the individual metal sheets are welded together. This can be done before, or after, priming and anodizing. Since pretreatment facilities have a size-limitation, it might be necessary to prime and anodize the individual sheets (with the to-be-welded area protected) before welding. A detailed analysis of the manufacturing process goes beyond the scope of the current research, but it needs to be noted that this is something to consider in subsequent research.

2.3 Damage tolerance aspects of FSWs

Before FSW-ed FMLs can be applied in aircraft structures, they have to be certified as DT. The first step in doing this is to get an overview of all the aspects that require special attention when considering the DT of FSWs. One of these aspects is the change in material properties at the location of the weld. Another important aspect to consider are the typical processing defects that may occur in FSWs, since this defines the starting point of the DT analysis in a later stage of the research. Before these subjects are discussed in more detail, a short overview of the FSW process and its definitions will be given.

2.3.1 Friction stir welding definitions

FSW is a process in which a non-consumable rotating tool is pressed against the surface of two abutting or overlapping plates [12]. This tool is composed of a specially shaped pin and shoulder and is translated along the joint. Due to the combined effect of tool rotation and translation the material around the tool softens because of the resulting frictional heat. It should be noted that the material does not melt, but is formed via plastic deformation.

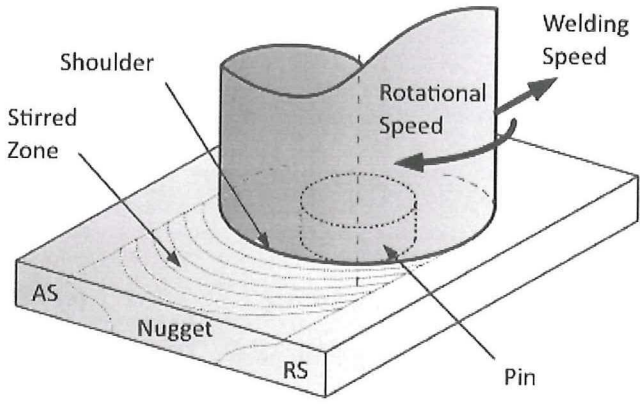

Figure 2.3: Scheme of the FSW process [13].

The side where the rotation and translation are in the same direction is called the Advancing Side (AS) of the weld. As can be seen from figure 2.3 the side where the rotation and translation are in the

opposite direction is called the Retreating Side (RS). From left to right one finds the Heat-Affected Zone (HAZ), Thermo-Mechanically Affected Zone (TMAZ), and the weld nugget. The HAZ is a zone that has a different microstructure than the parent material due to the elevated temperature, but has not experienced any plastic deformation. This is the case for the TMAZ. This zone normally consists of a region with elongated grains due to the tool rotation and a fully recrystallized region (the weld nugget).

2.3.2 Mechanical properties

A well known fact is that elevated temperatures and material deformation can influence the mechanical properties of metals. These changes in mechanical properties can also happen when a metal is FSW-ed. Studies have shown that the yield strength and ultimate strength of FSW-ed areas may be different from the parent material. While most of the studies indicate a significant reduction in mechanical properties [14, 15, 16], some studies show that the mechanical properties are similar to the parent material [17, 18]. Another factor is the directionality of the mechanical properties. Due to the rotational motion and the resulting wedge shape of the nugget, a difference can be observed between the properties at the root (bottom) and crown side (top) of the weld nugget [19]. A wider high yield strength-zone was observed at the crown side in Al2024-T3. Outside the nugget-zone, no differences were observed.

Differences were also observed in the crack growth rate. Moreira et al. [18] observed that the crack growth rate in FSW-ed parts of Al2024-T3 is lower than in the base material. This finding was not supported by the research by Ilman et al. [16] and Ali et al. [17]. They observed that the crack growth rate in the FSW-ed zone for this metal is higher than in the base material. One thing these results have in common is that the Paris constants used to calculate the crack growth rate are different from the ones used for the base material. Lemmen showed in his research that the actual situation is even more complicated due to the directionality of the welding process [19]. Crack growth rates differ depending on the distance from the weld center-line and the orientation of the crack towards this line. Experiments on Al2024-T3 samples showed that cracks grow faster in the welding direction than cracks that grow at an angle, and crack growth rates were lowest in the center of the weld and reached a maximum at a distance of 6.5 mm from the center line. The latter observation is in direct contrast with the findings from Ali et al., who observed that crack growth rates are highest in the center of the weld.

The differences in the obtained results can be explained based on the settings used in the FSW-process [7]. Tool shape, pressure, tilt angle, and rotation speed determine, for a large part, the amount of heat input in- and deformation of- the material. A difference in heat input and material deformation ultimately results in different local microstructures, causing a change in mechanical properties. Since the mechanical properties of the weld are highly dependent on the process settings it is necessary to determine them on a case-by-case basis.

2.3.3 Processing defects

Something which is also dependent on the process parameters, are the type of defects that occur in the weld. Typical defect categories found in FSWs are cold processing defects, hot processing defects, and geometry related defects [20].

Cold processing defects are formed at high travel speeds and low revolutions per minute. As can be seen from figure 2.4 three types of defects can occur at these process settings: a wormhole, chip lack of fill and scalloping.

A "wormhole" is a longitudinal tunnel formed at the AS of the weld, caused by insufficient consolidation of the material. Similar to this defect is the "chip lack of fill". This defect is a void

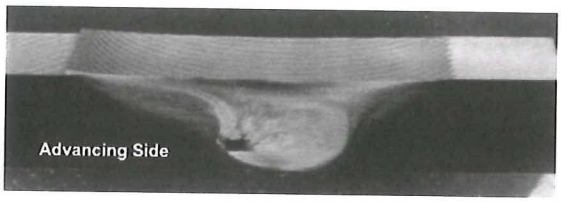

(a) Wormhole

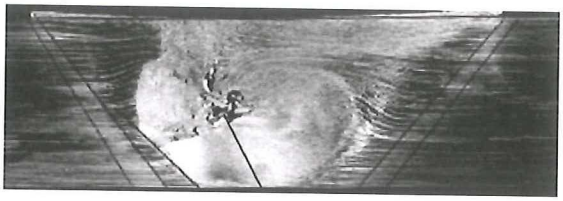

(b) Chip lack of fill

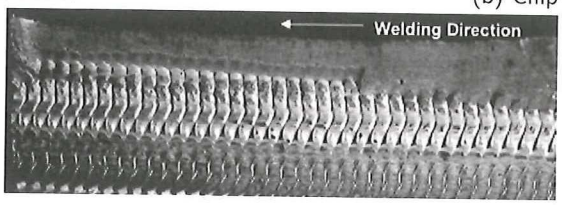

(c) Scalloping

Figure 2.4: Typical cold processing defects [20].

containing shards of metal. The "scalloping" defect is a series of small voids in the AS of the weld.

Contrary to cold processing defects, hot processing defects are formed at low travel speeds and high revolutions per minute. The seven typical hot processing defects are: kissing bond, weld flash, surface lack of fill, nugget collapse, surface galling, faying surface, and root flow defect. Figure 2.5 shows the four most visual defects.

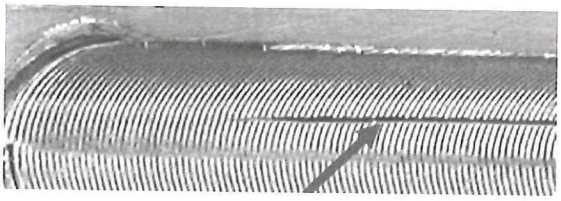

(a) Surface lack of fill

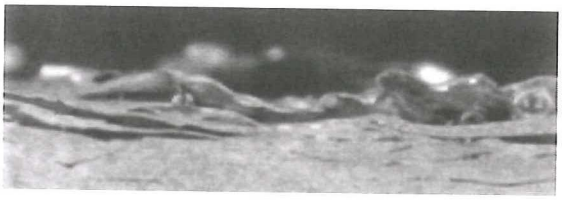

(b) Surface galling

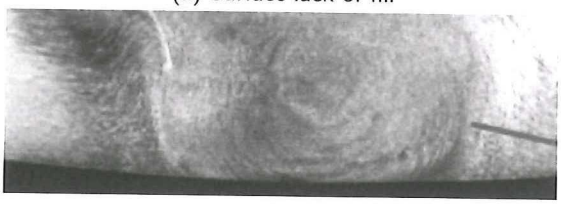

(c) Faying surface

(d) Root flow

Figure 2.5: Typical hot processing defects [20].

As can be seen from figure 2.5 the "surface lack of fill" is a longitudinal void formed at the surface of the weld. Another hot processing defect formed at the surface is, as can already be seen from the name, "surface galling". Galling and tearing of the top surface may occur beneath the pin tool if incorrect settings are used. The third defect, "faying surface", is a line of second phase particles located at the original faying surface. These second phase particles may reduce the mechanical properties of the joint if this phenomenon becomes excessive. The "root flow" defect is formed at the backside of the weld, where chevron shaped flow patterns are visible. When the nugget is formed insufficiently it is called "nugget collapse", and when remnants of the material are visible at the

advancing and retreating side of the weld, the "weld flash" defect has occurred. Most notable of all these defects is the "kissing bond", sometimes also referred to as "root flaw". The "kissing bond" is a partial remnant of the original but surface, consisting of metal oxide particles, below the stir zone.

Final category concerns the geometry related defects. Two FSW defects can be identified here, namely: lack of penetration and lack of fusion. The first, "lack of penetration", means that the weld nugget has not penetrated sufficiently in the material, leaving a remnant of the original faying surface. "Lack of fusion" also means that a remnant of the original faying surface is left, but this defect is caused by misalignment of the joint and the welding tool.

As will be shown in the next chapter, all of the defects mentioned in this section have to be considered in the DT certification of FSW-ed FMLs. One of the steps in the certification process is to determine the maximum damage that is expected in the structure. The defects mentioned in this section fall under manufacturing damage, which, next to service-induced damage, has to be included in the list of possible damage modes for the structure. From this list the worst-case damage modes are determined, which are then further analyzed and tested in the following steps. The manufacturing damage described above is especially important when considering Widespread Fatigue Damage (WFD). Some of the defects may occur at multiple locations in the weld causing the condition of Multiple Site Damage (MSD). A summary of all the defects, the required inspection methods and damage types (Single Site Damage (SSD) or MSD) is provided in table 2.1.

Table 2.1: Damage identification friction stir welding (Single Site Damage (SSD) and Multiple Site Damage (MSD)) [12, 21].

FSW defect	**Inspection method**	**Damage type**
Wormhole	Ultrasonic phased array	SSD
Chip lack of fill	Ultrasonic phased array	SSD
Scalloping	Visual	MSD
Nugget collapse	Ultrasonic phased array	SSD
Root flow	Visual	MSD
Weld flash	Visual	SSD
Surface lack of fill	Visual	SSD
Surface galling	Visual	MSD
Faying surface	Ultrasonic phased array	MSD
Kissing bond	Ionic eddy current	MSD
Lack of penetration	Ultrasonic phased array	SSD
Lack of fusion	Ultrasonic phased array	SSD

From this table it is clear that five defects can cause the condition of MSD. Of these five, only two cannot be detected by the naked eye. Since it is reasonable to expect that sheets with defects that are directly visible for the human eye will not be used in aircraft structures, only two types of defects remain. For both the "Faying Surface", and the "Kissing bond" it is necessary to know the typical defect size for further analysis at a later stage. This information is shown in table 2.2.

Table 2.2: MSD processing defect sizes.

FSW defect	**Typical defect size**	**Source**
Faying surface	0-50 μm	[17]
Kissing bond	0-24 μm	[22, 23, 24]

3

Damage Tolerance Certification

The first step in developing design principles for DT FSW-ed FMLs is to create a DT compliance plan. This compliance plan should ensure that the structure under consideration meets all the DT requirements set by aviation authorities. In order to ensure that all requirements are included in the plan, it is necessary to base this plan on DT evaluation methods accepted by the aviation authorities. Both the FAA and EASA developed their own DT evaluation methods; AC 25.571 for the FAA and CS 25.571 for EASA. Although small differences between the two methods exist, both are acceptable means to show DT of aircraft structures. For this research it was decided to use the method developed by the FAA, since this method provides a more detailed explanation of the different steps that have to be taken compared to EASA's method.

The DT evaluation described in AC 25.571 consists of four steps. First of these steps is to identify the structure under evaluation. After this step has been performed, a detailed description of the joint location and requirements for the joint should be available. Once the location of the structure has been identified, it is possible to determine the loading conditions and extent of damage that should be considered in the analysis, this is the area covered by the second step. The loading conditions and damage scenarios found in the second step serve as the basis for the structural tests and analyses performed under step three. Finally, the inspection and maintenance program can be constructed in the fourth step by using the outcome of the analyses and tests.

In this chapter a step-by-step guide to DT compliance will be presented, based on the four steps described above.

3.1 Identification of structure

Identifying the structure includes all steps from determining the location of the joint to setting requirements for the DT performance. Before the requirements can be set is necessary to know the location of the joint in the aircraft structure. This will provide information on which structural details should be considered in the analyses and tests. At this point it should be noted that it has to be checked whether the structure which is going to be altered, or that was designed, qualifies as DT. If the structure qualifies under the DT provisions stated in AC 25.611, the DT requirements can be established. If the structure, however, does not qualify a redesign is necessary.

Everything that has to be shown in the DT certification of the new joint is included in the

objective of the DT certification section, which is summarized as: *The damage-tolerance evaluation of structure is intended to ensure that, should fatigue, corrosion, or accidental damage occur within the LOV of the airplane, the remaining structure can withstand reasonable loads without failure or excessive structural deformation until the damage is detected.* [25] For the analyses and tests it is therefore necessary to know the design-limit loads, Design Service Goal (DSG) and Limit Of Validity (LOV). It has to be noted that multiple scenarios have to be considered in the analyses and tests. First of these scenarios is the single site damage scenario. This damage mode, which will be described in more detail in the following section, considers only a single growing crack in the structure. The second scenario involves cracking at multiple locations in the structure, which in the case of FSW-ed FMLs would be MSD. Both of these damage scenarios fall under the DT evaluation section of AC 25.571.

The third damage scenario that has to be evaluated is discrete source damage. The objective of this evaluation is summarized as: *The maximum extent of immediately obvious damage from discrete sources should be determined, and the remaining structure shown with an acceptable level of confidence, to have static strength for the maximum load (considered as ultimate load) expected during completion of the flight.* [25] From this it clear that the ultimate loads have to be determined. The ultimate loading conditions that have to be considered involve the maximum, normal, operating differential pressure, external aerodynamic pressure during 1g level flight combined with 1g flight loads and limit flight-maneuver loads.

3.2 Definition of loading conditions and extent of damage

For all the locations determined under step 1 the extent of damage and loading conditions have to be found. The extent of damage, which can be due to fatigue, corrosion or accidents, can be described based on the four parameters given in the guide in section 3.4. Damage mode and location should be determined from service experience and analysis. Since multiple damage modes are possible for all the different locations in the aircraft structure it is necessary to select the worst-case for further analysis and testing. The worst-case scenario is the damage mode with low initial residual strength, low detectability and high damage-extension rate. This process has to be followed for all three damage scenarios mentioned in the 'identification of the structure' step.

The repeated loads used in the analyses and tests have to be as defined in the loading, temperature and humidity spectra. If structural flexibility and loading rate are significant they have to be incorporated in the spectrum as well. When available, the loading spectrum should be based on measured statistical data of the type derived from government and industry load-history studies. This data is only available if the design is a type-design change and measurements were performed on the old aircraft structure by either government or industry. If this data is unavailable a conservative estimate of the expected use of the aircraft should be used.

3.3 Structural tests and analyses

Damage modes and loading conditions determined in the previous step can be used in the analyses and tests in the third main step. At this point it is necessary to show that the designed structure meets the DT requirements set under step 1. The general requirement for DT is that the structure with the extent of damage established for residual strength evaluation can withstand the specified design-limit loads. It should be noted, however, that besides the residual strength characteristics of the structure, the analyses and tests also provide information necessary for the development of the inspection and maintenance program.

Single site damage

In the 'Identification of the structure' step three different damage scenarios were introduced, that have to be considered in the DT analysis. Since each of these scenarios has a unique set of requirements for the analyses and tests, they will be treated separately in this section. The objective of the single site damage scenario is to show that damage would be detected before it reaches the value for residual strength evaluation, via analytical calculations supported by experimental data or via quantitative relations with structure already verified as DT. These two options are normally used in different design cases. Proving DT via analytical calculations is the best option in the case of a new type certificate, since no information on the DT performance of the structure is available. If this information is available, which is the case for a type design change, the method that uses quantitative relations is the best. In both cases the residual strength of the structure has to be evaluated after the test object has been subject to fatigue- or slow crack-growth- testing.

Since this compliance plan considers FSW-ed FMLs, where specific damage modes should be considered, the best option would be to choose slow-crack growth testing and analyses based on appropriate initial damage. The structure has to be designed to meet the requirement that design-limit loads can still be carried at the DSG. Analytical crack growth and residual strength calculation methods should be used to design the structure to meet this requirement. After the design has been completed it is necessary to test the structure for its crack-growth rate, and the residual strength at the DSG. For a new type certificate this implies testing the complete structure, whereas for a type design change testing at the component level and relating this to DT performance of the current structure would suffice.

Widespread fatigue damage

The second damage scenario that has to be analyzed and tested is WFD. This damage mode has to be evaluated since MSD (see section 2.3) is possible at the location of the welds. In this evaluation it has to be demonstrated that WFD is unlikely to occur up to the LOV of the aircraft via test evidence and analysis. More specifically, it has to be shown that the residual strength of the structure meets or exceeds the design-limit loads at the LOV.

Demonstration of these properties typically entails full-scale fatigue testing, followed by residual strength evaluation. In these laboratory tests structure representative of the type design is subjected to loading that simulates typical service operation. The test article may be the entire airframe or a portion of it. All test articles used should be conformed with 14 CFR 21.3, include all structural details as the designed structure, and be produced via the same manufacturing processes as the article to be simulated. The loads should be introduced as realistically as possible, which means that also loads due to secondary structure has to be incorporated in the test. If compromises are made finite element methods have to be used to prove the validity.

Since the structure has to be designed first it is necessary to demonstrate the DT properties analytically. Two methods are accepted for this analysis; fatigue crack initiation relying on fatigue data, and crack growth methods based on the fracture mechanics approach. From the section on the general damage scenario it is clear that in this case the fracture mechanics approach is the best way to demonstrate the DT properties. By designing the structure to have sufficient strength to carry the design-limit loads at the LOV it can be demonstrated that all requirements are met. This design concept should then be put to the test in the following step.

As with the tests for the general damage scenario, a differentiation has to be made between the type of compliance projects. The scope of the full-scale fatigue test article, namely, depends on the type of certification project. For a new type certificate, testing a complete airframe would be the best option since multiple WFD-susceptible areas need to be analyzed. This is different from a type design change, where the test article only consists of the design change and any structure that is

negatively affected by this change. If existing relevant data (amendment 25-96 or later) is available, no full-scale testing may be required, provided that the type-certificate holder demonstrates that the design change and original structure is free from WFD up to the LOV. This means that if this data is available, testing at the component level will suffice. The final tests that should be considered are repairs. If the repairs are published, fatigue and damage-tolerance analysis that correlates to results of full-scale fatigue testing can be used to demonstrate freedom from WFD up to the LOV. Non-published repairs, that are also not included in FAA-approved published data, require either full-scale testing or a proposal analysis method that compares the original type design to the repair.

From the tests it is possible to determine the average time to develop WFD. This number is denoted by $WFD_{averagebehavior}$ and is expressed in flight cycles or hours. Results of one full-scale fatigue test can be used as proof for this number. All of the inspection and maintenance tasks are derived from this number. The inspection starting point (ISP) is determined by dividing $WFD_{averagebehavior}$ by three if inspections are effective in detecting damage. The structural modification point (SMP) is the same number divided by two if inspections are effective, or divided by three if inspections are not effective. Based on these numbers it is possible to determine the required length of the tests. If a test of three times the LOV is done without the occurrence of WFD, no WFD-related mandatory maintenance actions are required. For repairs and type design changes a test duration of three times the remaining life of the structure is advised.

After the fatigue test is completed it is necessary to determine the residual strength of the structure. It has to be shown that at three times the LOV the structure can still withstand the design-limit loads. Residual strength can either be determined analytically or via testing. The first option, analytic determination, requires teardown inspections and provides detailed information about the crack size and distribution. Testing allows exact determination of the residual strength, but does not provide information on how many more cycles are required for WFD to form.

If it is demonstrated that the strength is equal to, or greater than, required, the final LOV can be set equal to the candidate LOV. If the strength is less than required at three times the LOV two options are possible: maintenance actions or design changes. Changing the design makes it possible to increase the residual strength to the required level to avoid maintenance tasks. If it is decided to keep the current design, maintenance tasks have to be performed at the already mentioned intervals. The final LOV, including possible inspections, modifications, and replacements of structure, stated as total accumulated flight cycles or hours has to be included in the ALS.

Discrete source damage

The final damage scenario that has to be analyzed is discrete source damage. In this analysis it has to be shown that, with the extent of damage established under the previous step, the structure can still withstand the ultimate loads expected during the remainder of the flight. Four different loading conditions have to be considered in the analytic calculations [25]:

I. At the time of the incident:

   1 *Maximum, normal, operating differential pressure multiplied by 1.1, plus the expected aerodynamic pressure during 1g level flight combined with 1g flight loads.*

   2 *Any maneuver or flight-path deviation caused by the incident during 1g level flight (include possible damage to flight controls and pilot action).*

II. Following the incident:

   3 *Seventy percent limit flight-maneuver loads and, separately, fourty percent of the limit gust velocity (vertical and lateral) at the specified speeds, each combined with the maximum appropriate cabin differential pressure including the expected aerodynamic pressure.*

4 *It has to be shown that no flutter occurs up to V_D/M_D following any change in stiffness of the structure.*

3.4 Damage tolerance compliance guide

All of the information in this chapter applied to FSW-ed FMLs leads to the following step-by-step DT compliance guide:

1. Determine the location of the joint in the aircraft structure.
2. Obtain a detailed view of all structural details at the location of the joint.
3. Check if the structure qualifies under the DT provisions stated in AC 25.611.

If the structure qualifies under the provisions go to step 4, *elseif* redesign the structure to meet the provisions.

4. Determine the values for the following variables:
   (a) Design-limit loads
   (b) Design service goal
   (c) Limit of validity
5. Develop a list of damage modes for all three damage scenarios in terms of the following parameters:
   (a) Detectability with the inspection technique used
   (b) Initially detectable crack size
   (c) Residual strength of the structure
   (d) Likely damage-extension rate
6. Select the worst-case damage modes from the list for all three damage scenarios.
7. Determine the loading conditions for the joint.
8. Determine the DT performance of the structure for the first damage scenario (single site damage) analytically.
   (a) Calculate the crack growth up to the required number of flight cycles or hours (DSG*3 if maintenance tasks and inspections are unwanted, DSG<..<DSG*3 if these actions are acceptable)
   (b) Calculate the residual strength of the structure at the same number of flight cycles or hours

If the residual strength is found to be equal to, or greater than, the design-limit loads continue with step 9, *elseif* redesign the structure to meet the set requirements and go back to step 8.

9. Determine the DT performance of the structure for the second damage scenario (WFD) analytically.

(a) Calculate the crack growth up to the required number of flight cycles or hours (LOV*3 if maintenance tasks and inspections are unwanted, LOV<..<LOV*3 if these actions are acceptable)

(b) Calculate the residual strength of the structure at the same number of flight cycles or hours

If the residual strength is found to be equal to, or greater than, the design-limit loads continue with step 10, *elseif* redesign the structure to meet the set requirements and go back to step 9.

10. Determine the DT performance of the structure for the third damage scenario (DSD) analytically.

    (a) Calculate the residual strength of the structure

    (b) Calculate the loads at maximum, normal, operating differential pressure multiplied by 1.1, plus the expected aerodynamic pressure during 1g level flight combined with 1g flight loads at the time of the incident

    (c) Calculate the loads due to any maneuver or flight-path deviation caused by the incident during 1g level flight

    (d) Calculate seventy percent of limit flight-maneuver loads and, separately, fourty percent of the limit gust velocity (vertical and lateral) at the specified speeds, each combined with the maximum appropriate cabin differential pressure including the expected aerodynamic pressure following the incident

    (e) Calculate the flutter at V_D/M_D following any change in stiffness of the structure

If the residual strength of the structure is equal to, or greater than, the ultimate loads and no flutter occurs, continue the analysis, *elseif* redesign the structure to meet the set requirements and go back to step 10. *If* the structure under consideration is a type design change *and* information on the DT performance of the structure is available continue with step 11, *elseif* continue with step 12.

11. Perform slow-crack growth and residual strength tests on FSW-ed FML specimens (SSD) and relate the performance to the known materials.

    (a) Determine the crack growth up to the required number of flight cycles or hours (DSG*3 if maintenance tasks and inspections are unwanted, DSG<..<DSG*3 if these actions are acceptable)

    (b) Determine the residual strength at the same number of flight cycles or hours

    (c) Establish quantitative relations between the crack growth rate and residual strength of normal FMLs and FSW-ed FMLs

    (d) Determine the crack growth and residual strength of the complete FSW structure under consideration based on the developed quantitative relations and the DT performance of the old structure

If the residual strength is found to be equal to or greater than the design-limit loads continue with step 13, *elseif* redesign the structure to meet the set requirements and go back to step 8.

12. Perform slow-crack growth and residual strength tests on a full scale fatigue test article.

    (a) Determine the crack growth up to the required number of flight cycles or hours (DSG*3 if maintenance tasks and inspections are unwanted, DSG<..<DSG*3 if these actions are acceptable)

(b) Determine the residual strength at the same number of flight cycles or hours

If the residual strength is found to be equal to or greater than the design-limit loads continue with step 14, *elseif* redesign the structure to meet the set requirements and go back to step 8.

13. Perform slow-crack growth and residual strength tests on FSW-ed FML specimens (MSD) and relate the performance to the known materials.

    (a) Determine the crack growth up to the required number of flight cycles or hours (LOV*3 if maintenance tasks and inspections are unwanted, LOV<..<LOV*3 if these actions are acceptable)

    (b) Determine the residual strength at the same number of flight cycles or hours

    (c) Establish quantitative relations between the crack growth rate and residual strength of normal FMLs and FSW-ed FMLs

    (d) Determine the crack growth and residual strength of the complete FSW structure under consideration based on the developed quantitative relations and the DT performance of the old structure

If the residual strength is found to be equal to or greater than the design-limit loads at LOV<..<LOV*3 continue with step 15, *if* the residual strength is found to be equal to or greater than the design-limit loads at LOV*3 continue with step 16, *elseif* redesign the structure to meet the set requirements and go back to step 9.

14. Perform a full-scale fatigue tests consisting of either the complete airframe or a portion of it.

    (a) Test the article up to the required number of flight cycles or hours (LOV*3 if maintenance tasks and inspections are unwanted, LOV<..<LOV*3 if these actions are acceptable)

    (b) Determine the residual strength at the same number of flight cycles or hours either analytically or via residual strength testing

If the residual strength is found to be equal to, or greater than, the design-limit loads at LOV<..<LOV*3 continue with step 15, *if* the residual strength is found to be equal to, or greater than, the design-limit loads at LOV*3 continue with step 16, *elseif* redesign the structure to meet the set requirements and go back to step 9.

15. Include the following in the ALS:

    (a) LOV stated as total number of flight cycles/hours

    (b) Maintenance tasks at $WFD_{averagebehavior}/2$ if inspections are effective in detecting damage or $WFD_{averagebehavior}/3$ if inspections are ineffective

    (c) Inspection tasks at $WFD_{averagebehavior}/3$

16. Include the following in the ALS:

    (a) LOV stated as total number of flight cycles/hours

This plan will be used as the basis for the development of the design principles and concepts for FSW-ed FMLs throughout the rest of the research.

4

Damage Tolerance Analysis Methodology

In order to develop the design concepts and principles for the application of FMLs with FSW-ed aluminum sheets in aircraft structures it is necessary to have methods available to analyze the DT characteristics of the material. From the study on the DT certification procedure it is clear that both the crack growth in, and residual strength of, the structure should be analyzed. This chapter will present analytical methods that can be used to predict these structural characteristics for all of the damage modes that could be encountered in FSW-ed FMLs. The first section, section 4.1, covers the crack initiation and growth for SSD. Analytical methods for calculating the residual strength for this damage mode are presented in section 4.2. The other damage mode, MSD, requires a different approach. Crack initiation and growth models for this mode are given in section 4.3, and residual strength prediction methods in section 4.4.

4.1 Single site damage crack initiation and growth

Crack initiation and growth in FMLs is a subject that has been studied by multiple researchers over time. Homan [27] investigated fatigue crack initiation in these materials. His research showed that fatigue initiation was determined solely by the stress cycles in the metal layers. If the stresses in the metal layers are known it is thus possible to calculate the crack initiation period in the same way as for standard metals. The stress system in the metal layers can be calculated using Classical Lamination Theory (CLT).

Homan's model was recently improved by Spronk et al. [28], by including the effect of rotated thermal expansion for the different layers and providing a method to determine the right, thermal stress dependent, stress concentration factor. This method finally allowed for good predictions of the crack initiation time in FMLs.

Once the cracks have formed and the initiation period has been calculated, it is necessary to determine the crack growth in the material. An analytical model for Constant Amplitude (CA) fatigue crack propagation was developed by Alderliesten [29]. This model is based on the stress intensity at the crack tip in the aluminum layers, meaning linear elastic fracture mechanics can be used to calculate the crack growth rate. One of the limitations of this model is that it can only be used for through-cracks (equal crack length in all of the metal layers). Yang et al. [30] further improved this model by allowing it to be used for determining the crack growth rate for surface- and

part-trough cracks as well.

Since the material will undergo Variable Amplitude (VA) loading in real life it is essential to have a model that captures this effect. Khan et al. [31] extended the method from Alderliesten to predict fatigue crack growth under VA loading. The results of their research showed that the model is capable of predicting the crack growth rate reasonably well for steep load spectra, whereas a mismatch is obtained when flat load spectra are considered. Although this is something that still needs to be improved it was decided to use this model in the current research, since it is the only readily available model that captures all required aspects and shows good results for most load spectra.

One of the things all of these researches have in common is that the tests and analyses were performed on FMLs without any anomalies, such as FSWs. Although the methods thus do not apply directly to the subject under investigation, they do provide a solid basis for further development.

The main difference between the case with, and without, FSWs is the introduction of a zone with (depending on the welding settings used) different mechanical properties [14, 15, 16, 17, 18], residual welding stresses [17, 7], and differing crack growth rates [16, 17, 18]. Since these changes will have a minor impact on the applicability of the aforementioned analysis methodologies, only sections of the theory that are affected will be discussed in this report. The different mechanical properties and residual welding stresses are dealt with in the section on far-field metal layer stress, whereas the difference in crack growth rates is discussed in the final calculation step: determining the crack growth rate.

4.1.1 Far-field metal layer stress

One of the changes induced by the FSW-ed zone is the difference in mechanical properties compared to the standard metal. Although these changes are important to consider, they do not influence the stress in the metal layers. The far-field stresses are only dependent on the stiffness of the material, the applied stress, the coefficients of thermal expansion and possible other residual stresses. Since the stiffness and thermal expansion of the FSW-ed material are the same as that of the parent material, it is possible to conclude that the differing mechanical properties do not influence the stress level in the welded layer.

The residual welding stresses, on the other hand, do influence the stress level in the individual layers. Without the FSW, the stresses in these layers are the sum of the applied stress and the residual curing stress only. The residual welding stresses, however, are a third contributor to the total stress level. As can be seen from equation 4.1 the residual welding stresses have to be added as a separate contribution to the total stress level in the metal layer.

$$\sigma = \bar{Q}(\bar{\varepsilon}^0_{tot} + z\kappa_{tot} - \bar{\alpha}\Delta T) + \sigma_{res} \tag{4.1}$$

In this equation $\bar{Q}$ is the stiffness matrix of the layer in laminate coordinates, z the distance to the mid-plane of the laminate and ΔT the difference between curing and operating temperature. A (possibly) better way to include the residual welding stresses in the calculations would be to add them to the load matrix in the equation for mid-plane strain, $\bar{\varepsilon}^0_{tot}$, and curvature, κ_{tot}, which, for a standard FML, takes the form of equation 4.2 [28].

$$\begin{Bmatrix} \bar{\varepsilon}^0_{tot} \\ \bar{\kappa}_{tot} \end{Bmatrix} = \begin{bmatrix} a & b \\ b & d \end{bmatrix} \begin{Bmatrix} N + N^{th} \\ M + M^{th} \end{Bmatrix} \tag{4.2}$$

Here N and M are the load and bending moments for the applied load and the fictional thermal forces (th). By adding the residual welding stresses in the form of a load matrix, it is possible to automatically include the effect of the directionality of these stresses [19]. It needs to be noted that, in this form, the model is only valid for the case where all the metal layers are FSW-ed and have the

weld under the same angle. For other cases an adjusted version of this model has to be developed and therefore, for the moment, the residual welding stresses have to be added as a separate contribution to the layer stress as in equation 4.1.

4.1.2 Crack growth rate

All of the methods presented in this section can further be applied directly to the case of a FSW-ed FML, except for the final calculation step. In this final step the crack growth rate is calculated using equation 4.3.

$$\frac{da}{dn} = C_{cg}\Delta K_{eff}^{n_{cg}} \tag{4.3}$$

This equation is a relation between the crack growth rate $\frac{da}{dn}$ and the effective stress intensity range ΔK_{eff} based on the experimentally obtained constants C_{cg} and n_{cg}. Since these constants for FMLs with and without FSW-ed sheets may be different, it is necessary to determine these constants experimentally and apply them in subsequent crack growth calculations.

Once the constants have been obtained it is possible to calculate the crack growth for both through-cracks and part-through-cracks using the models presented in this section. The only step left for SSD is then to determine the residual strength of the fatigued structure.

4.2 Single site damage residual strength

The calculation of the residual strength of FMLs with SSD is something that requires different theories for different damage scenarios. A well known method for predicting the residual strength of center cracked FML panels is the K_R-curve method [32]. Although this method can be used to accurately predict the residual strength, its applicability is limited to panels with accidental damage, meaning a different method is required to determine the residual strength of fatigue cracked panels. A methodology that can be applied in these cases was developed by Müller [33]. This method (here referred to as the Damage Ratio (DR) method) is based on the fraction of cracked metal over pristine material. Since both methods provide valuable and necessary insight in the DT performance of the structures under consideration, both models will be discussed in this chapter. The DR method can, however, also be applied to predict the residual strength of panels with MSD. Since SSD is a simplified case of MSD, the discussion of the DR theory is left for the section on MSD residual strength.

4.2.1 K_R-curve method

To successfully predict the residual strength of fractured FMLs, it is necessary to have a criterion independent of the width of test specimens and the size of the cracks. The K_R-curve approach meets both of these criteria, making it a suitable method for designing FML structures. Although it is not possible to predict the residual strength of fatigued specimens (no stable crack extension occurs), the R-curve approach can be used to determine the residual strength of specimens with accidental damage [32].

The current approach is based on the balance between energy release rate, G, and crack resistance, R, of the material. Figure 4.1 illustrates the basic concept of the method. Note that in the figure stress intensity units K_G and K_R are used in stead of the energy release rate and crack resistance. These stress intensity units are directly related to the energy release rate and crack resistance via the Young's modulus of the material; a more detailed explanation of these variables can be found in de Vries [32].

When a center crack of length $2a_0$ is present in the material crack growth commences at stress σ_i, shown as point A in figure 4.1. At that point the initial crack (of length $2a_0$) has grown to the length $2_a(A)$. No further crack growth happens at this stress level, because for cracks larger than this length the crack resistance is bigger than the energy release rate. Once the stress level is raised, the crack is allowed to grow to point B. Stable crack extension occurs until point C is reached. This is the point where the stress level has reached the critical stress level, σ_c. At this point K_G is larger than K_R no matter what the crack length is, implying that crack growth has become unstable.

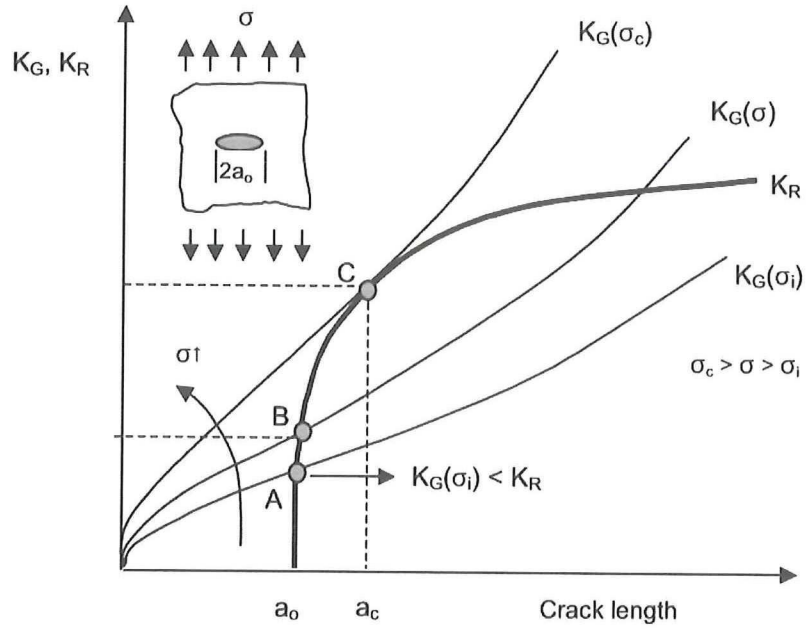

Figure 4.1: Concept of the K_R-curve and crack driving force curves for thin center cracked plates [32].

K_R-curves can thus be matched with the K_G-curves to determine the load that causes unstable crack propagation [34]. To determine the critical load the origin of the K_R-curve is positioned at the initially assumed crack length, a_0. By drawing different K_G-curves it is then possible to determine the load that causes unstable crack propagation (the residual strength) by finding the unique curve that develops tangency with the K_R-curve. The crack length at which unstable crack propagation starts is called the critical crack length, a_c.

The K_G-curves can be calculated using equation 4.4.

$$K_G = \sqrt{\frac{1}{cos(\pi \frac{a}{W})}} \sigma \sqrt{\pi a} \tag{4.4}$$

In this equation a is the half crack length, W the width of the test specimen, and σ the applied stress.

By repeating the aforementioned procedure for multiple assumed crack lengths it is possible to determine a relationship between the residual strength of the material and the initial crack length. This relationship can be used directly to determine the residual strength of a center cracked panel if

the crack length is known. All of this can only be applied to FSW-ed FMLs if the K_R-curve of the material is known. For this method to work it is therefore necessary to experimentally determine the K_R-curve.

4.3 Multiple site damage crack initiation and growth

When it comes to calculating the crack initiation and growth rates for FMLs with MSD, one finds that the methods that can be used to do this are fully based on the principles used for FMLs with SSD. The initiation period, for example, is again only dependent on the stresses in the metal layers and can therefore be calculated using the method from Homan [27]. Whereas this is something that can be applied directly, the actual calculations for the Stress Intensity Factor (SIF) require a modified approach. In the work from Yang et al. [30] it was shown that it is possible to predict the crack growth rate in FMLs for both MSD trough-thickness cracks, and MSD partial-through cracks using their model. Their approach is unique in the fact that weight functions are used to model the effect of multiple site cracking. A different approach was suggested by Wang [36]. His hypothesis is that additional cracks can be treated as negative stiffeners in the SIF calculations.

4.3.1 Weight function method

Compared to the method from Alderliesten [29], the main difference in the weight function method can be found in the expression for the effective SIF.

$$K_{tip} = (K_{farfield} - K_{opening})(1 - \beta_f)f_0 \tag{4.5}$$

As can be seen from equation 4.5, the SIF at the crack tip here is the sum of the far-field SIF ($K_{farfield}$) and the crack-opening SIF ($K_{opening}$) multiplied by a non-dimensional fibre-bridging factor, β_f, and a geometrical correction factor, f_0.

The method presented by Yang et al. can be used to predict the crack growth rate for part-through cracks because it incorporates the effect of bending stresses that occur due to the shift in neutral line position. Since these bending stresses are directly applied to the different metal layers, they have to be included in the equation for the far-field SIF.

$$K_{farfield} = (\sigma_{al} + \sigma^b{}_{al})\sqrt{\pi a} \tag{4.6}$$

Here σ_{al} is the stress in the aluminum layer, σ^b_{al} the stress caused by secondary bending, and a the total crack length.

The crack-opening SIF is defined as shown in equation 4.7.

$$K_{opening} = \sigma_{al,op}\sqrt{\pi a} \tag{4.7}$$

Here $\sigma_{al,op}$ is the crack-opening stress, which can be determined using an emperical relation based on the applied stress ratio in the aluminum layers, as presented in [30].

Due to the multiple site fatigue damage it is necessary to take into account the geometry and configuration of the specimen. This is done by applying the non-dimensional SIF (f_0), shown in equation 4.8.

$$f_0 = \int_{a_0}^{a} \sigma_0(x)\frac{m_0(a,x)}{\sqrt{\pi a}}dx \tag{4.8}$$

In this equation σ_0 is the stress on the crack face and m_0 the weight function, which can be calculated from equation 4.9.

$$m_0(a,x) = 2\sqrt{\frac{a}{\pi(a^2 - x^2)}} \tag{4.9}$$

The other non-dimensional SIF (f_{br}) can be determined from equation 4.10.

$$f_{br} = \int_0^a \sigma_{n,br,al}(x)\frac{m_{br}(a,x)}{\sqrt{\pi a}}dx \tag{4.10}$$

Here $\sigma_{n,br,al}$ is the bridging stress on the crack face in the metal layers and m_{br} the weight function. Yang et al. also included the exact weight function for a periodic array of collinear cracks in a sheet. This equation, where s is the distance between the centers of the starter notches, is shown in the form of equation 4.11.

$$m_{br}(a,x) = cos(\frac{\pi x}{2s})\sqrt{\frac{\frac{2s}{\pi a}tan(\frac{\pi a}{2s})}{sin^2(\frac{\pi a}{2s}) - sin^2(\frac{\pi x}{2s})}} \tag{4.11}$$

This method showed good agreement with experimental results for Glare specimens with multiple-site fatigue through-cracks under different stress levels. The same is true for Glare specimens with multiple site fatigue surface cracks. Predictions from the model for lead cracks match closely with the obtained experimental results. Although some discrepancies exist for non-lead cracks, it is expected that this method can be used to predict the crack growth rates for FSW-ed FMLs with MSD if the right material parameters are used.

4.3.2 Negative stiffener method

A different approach to the MSD problem is the method suggested by Wang [36]. In this research it is hypothesized that additional cracks can be treated as 'negative stiffeners'. Rans et al. [37] developed an analytical method to determine the SIF in cracked FML panels with stiffening elements. In this approach the effect of the stiffener is superimposed over the farfield and bridging SIF. Instead of the positive contribution from the stiffening element, the additional cracks act as 'negative stiffeners' to the SIF, as shown in equation 4.12.

$$K_{tip} = K_{farfield} - K_{bridging} + K_{negative,stiffener} \tag{4.12}$$

While this method looks promising, it is still under development at this moment and can therefore not be used in the current research.

4.4 Multiple site damage residual strength

Residual strength evaluation for structures or specimens with MSD is something that requires a different approach from SSD residual strength evaluation. Especially for relatively complex materials, such as FMLs, in which a large variety of damage situations can occur, it is difficult to find an approach that covers all of the different configurations.

Three of the more simple damage configurations are shown in figure 4.2. In all of the examples in this picture, the metal layers are fully cracked or damaged.

For the first and second situation from the left, an analytical residual strength evaluation method was developed by van der Jagt [38]. In this method the notch is treated as a location of strain concentration. By determining the stress concentration factor (which is used as a strain concentration factor) for a specific notch type, the strain distribution in the laminate is determined. Once the calculated strain reaches the maximum strain for the specific laminate, the force on the laminate

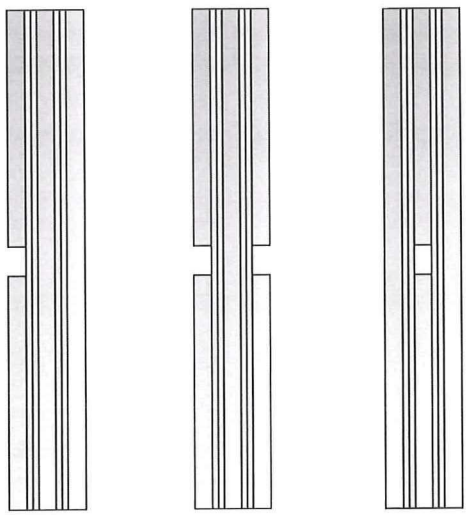

(a) One outer (b) Both outer (c) Center

Figure 4.2: Three possible damage situations in FMLs (fully cracked layers).

is calculated and assumed to be equal to the residual strength of the laminate. A major downside of this method is that, at the moment, it can only be used for very specific cases, since the strain concentration factors were adjusted manually based on experimental results. Another thing to note is that this method does not allow residual strength evaluations for partially cracked layers or layers cracked at multiple locations. It is therefore safe to say that a different method is preferred.

The only method that meets all the requirements is the DR method from Müller [33] and de Rijck [35].

4.4.1 Damage ratio method

Predicting the residual strength of fatigue cracked FMLs with MSD is something that requires a different approach from FMLs with SSD. A well proven model to do this was developed by Müller [33]. This model is based on the area fraction of broken metal layers in the laminate. If this fraction is known from the crack growth calculations it is possible to predict the residual strength of the laminate using this theory.

De Rijck [35] used this approach to calculate the residual strength of fatigue cracked riveted FML lap-joints. His results showed that the model can closely predict the residual strength of fatigue cracked Glare laminates.

The model assumes a linear degradation of the residual strength based on the fraction of cracked aluminum layers (the Damage Ratio). For standard FMLs this means that, if the crack size and laminate properties are known, it is possible to calculate the residual strength. A small adjustment has to be made to the model to incorporate the effect of FSW-ed metal layers. Since these layers may have a different ultimate strength from the parent material it is necessary to include the contribution from these layers to the laminate strength separately. The final result of this modification is shown in equation 4.13.

$$\sigma_{res} = \sigma_{u,lam} - MVF\frac{A_{al,cracked}}{A_{al,pristine}}\sigma_{u,al} - WVF\frac{A_{FSW,cracked}}{A_{FSW,pristine}}\sigma_{u,FSW} \tag{4.13}$$

In this equation $\sigma_{u,lam}$ is the ultimate strength of the intact laminate, $A_{cracked}$ the area of cracked material, $A_{pristine}$ the area of intact material, and σ_u the ultimate strength for the material (where the material is indicated with al for aluminum and FSW for welded aluminum). The Metal Volume Fraction (MVF) and Weld Volume Fraction (WVF) can be calculated from equations 4.14 and 4.15 respectively.

$$MVF = \frac{\sum_{i=1}^{n} t_{al,i}}{t_{lam}} \tag{4.14}$$

$$WVF = \frac{t_{FSW}}{t_{lam}} \tag{4.15}$$

Here $t_{al,i}$ is the thickness of aluminum layer i, t_{FSW} the thickness of the FSW-ed layer, and t_{lam} the total thickness of the laminate. The ultimate strength of the laminate can be calculated from the material properties of the individual constituents using equation 4.16.

$$\sigma_{u,lam,0} = V_{al} \cdot \sigma_{u,al} + V_{FSW} \cdot \sigma_{u,FSW} + V_{pre,0} \cdot \sigma_{u,pre,0} + V_{pre,90} \cdot \sigma_{u,pre,90} \tag{4.16}$$

Here V is the volume fraction of the material, $pre, 0$ is prepreg with fibres in the $0°$ direction, and $pre, 90$ prepreg with fibres in $90°$ direction.

Although it is possible to determine the residual strength of fatigue cracked FSW-ed FMLs using equation 4.13, presenting the results requires a 3-dimensional graph. Since it may be difficult to interpret results from 3D graphs, a better solution would be to capture both DR's in one effective damage ratio in the form of equation 4.17.

$$DR_{eff} = \frac{WVF \cdot \sigma_{u,FSW}}{MVF_{eff} \cdot \sigma_{u,eff}} DR_{FSW} + \frac{MVF \cdot \sigma_{u,al}}{MVF_{eff} \cdot \sigma_{u,eff}} DR_{al} \tag{4.17}$$

By using the effective DR instead of its individual constituents, it is possible to present all of the results in a 2-dimensional graph. The final form of the equation for the residual strength then becomes equation 4.18. ($\sigma_{m,lam}$ is the calculated value of the residual strength when all metal layers, including the FSW-ed layer, are fully cracked)

$$\sigma_{res} = \sigma_{u,lam} - (\sigma_{u,lam} - \sigma_{m,lam}) \cdot DR_{eff} \tag{4.18}$$

5

Damage Tolerance Performance of Friction Stir Welded Fibre Metal Laminates

One of the most important steps in the DT compliance plan is the establishment of quantitative relations between the DT performance of FSW-ed FMLs and standard FMLs. These relations can be used directly in designing the concepts for FMLs with FSW-ed metal sheets. Experimental results from research on the DT performance of FMLs needs to be coupled to experimental results in the same area for FSW-ed FMLs. The fatigue crack growth and residual strength data for standard FMLs is already available from work done by other researchers, this allows for the current program to be fully focused on FSW-ed FMLs. This program will, along with its results, be presented in the current chapter. The chapter is divided in the sections SSD crack initiation and growth, MSD crack initiation and growth and MSD residual strength. Each of the sections is further divided in three subsections, which respectively describe the program objective, the specimen geometry and test-set up, and the measurements and observations.

5.1 Single site damage crack initiation and growth

5.1.1 Program objective

The purpose of the SSD crack initiation and growth test program was to develop quantitative relations between the crack growth rate in FSW-ed Glare and standard Glare for through cracks. Since it is essential to obtain data independent of the specimen geometry, the crack growth rate has to be related to the stress intensity factor at the crack tip. Although it would have been ideal to measure the growth rate for the full range of SIFs typically encountered in aircraft structures, only a small part could be measured due to the limited availability of FSW-ed aluminum. In order for the data to be more meaningful, measurements were performed at different stress levels; this stretched the range of SIFs at which crack growth data could be obtained. The obtained data could further be used to (partially) validate the analytical methodologies from chapter 4.

5.1.2 Specimen geometry and test set-up

All of the specimens used in the testing program were made of Glare 3-3/2-0.4. The reason for choosing grade 3 as the basis for this research is that it is (due to its excellent fatigue and impact properties) already used as fuselage skin in existing aircraft [35]. For the same reason, Glare 4B could have been chosen, since this grade is typically applied in the rear of the fuselage. This version of Glare has a higher strength than Glare 3 in the 90° direction, which means the impact of the welded region on the residual strength will be smaller. In order to judge the initial viability of the idea of FSW-ed FMLs in terms of DT it is necessary to evaluate the worst-case scenario, meaning grade 3 was the logical choice.

The material for the test specimens consists of 3 aluminum 2024-T3 layers of 0.4 mm thick and 4 S2-glass FM94-prepreg layers of 0.133 mm thick. A general example of the laminate stacking sequence is shown in figure 5.1.

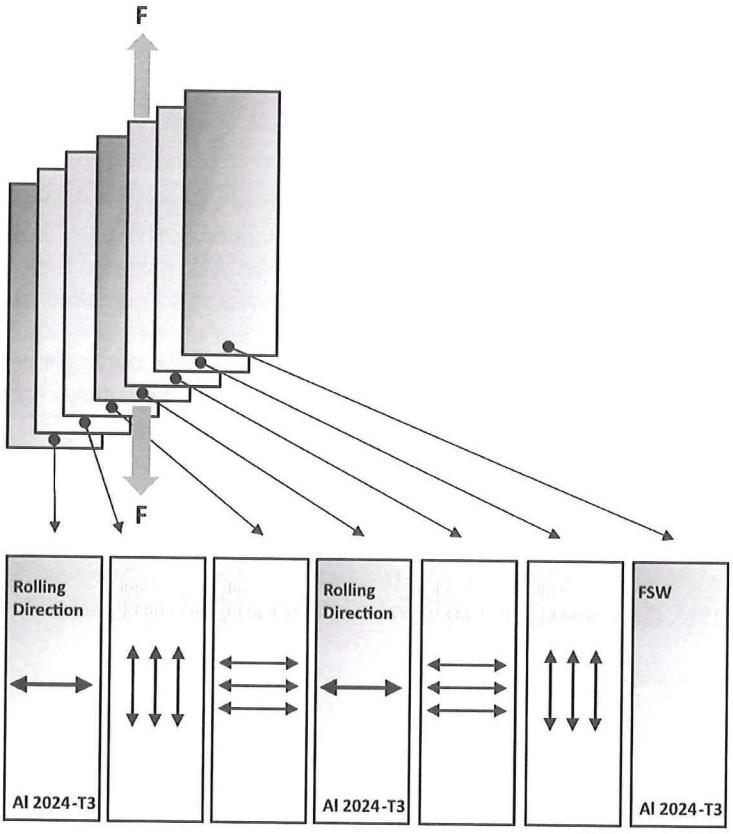

Figure 5.1: General example of laminate stacking sequence. (Image edited from [9])

As can be seen from this figure the outer prepreg layers are orientated at a 90° angle to the rolling direction of the aluminum layers and the inner prepreg layers at a 0° angle. To make the best use of the limited available FSW-ed aluminum, only 1 layer of it is used in each of the specimens. This decision will not influence the validity of the test results as long as the FSWs in the final design concept will not be in each others zone of influence (i.e. crack growth rates and residual strength are

not negatively affected by the inter-weld distance). De Vries [32] observed that the residual strength of a spliced FML panel stayed constant in the range of 12.7 to 50.8 mm for the splice distance, indicating that an inter-weld distance in this range should ensure no mutual influence. The only thing that is variable in the material stacking sequence is the position of the welded sheet; this sheet can either be placed in the outer (as shown in figure 5.1) or the center layer (which is the middle layer of the laminate shown in the figure).

All of the traditional Glare production steps have been followed in producing the specimens, except for priming and anodizing of the FSW-ed sheets. The sheets were directly stacked into the laminate after etching. In reality, priming is applied to prevent the aluminum sheets from re-oxidizing after they have been etched. If the time between etching and lay-up is small, it is possible to omit this step since there is not enough time for the aluminum to re-oxidize. Anodization could be skipped because this is normally done to improve the corrosion-resistance of the laminate. Since all of the specimens were tested under laboratory conditions corrosion-prevention was unnecessary.

For the SSD crack initiation and growth tests it was decided to keep the FSW-ed sheet as the outer layer to allow accurate monitoring of the crack growth in the weld. As can be seen from figure 5.2, an 11 mm long through slit was machined in the center of the weld (SSD1 and SSD2) to facilitate precracking. The reason for choosing this specific location for crack measurement was that this is the area where the crack growth rate in the weld is highest [17].

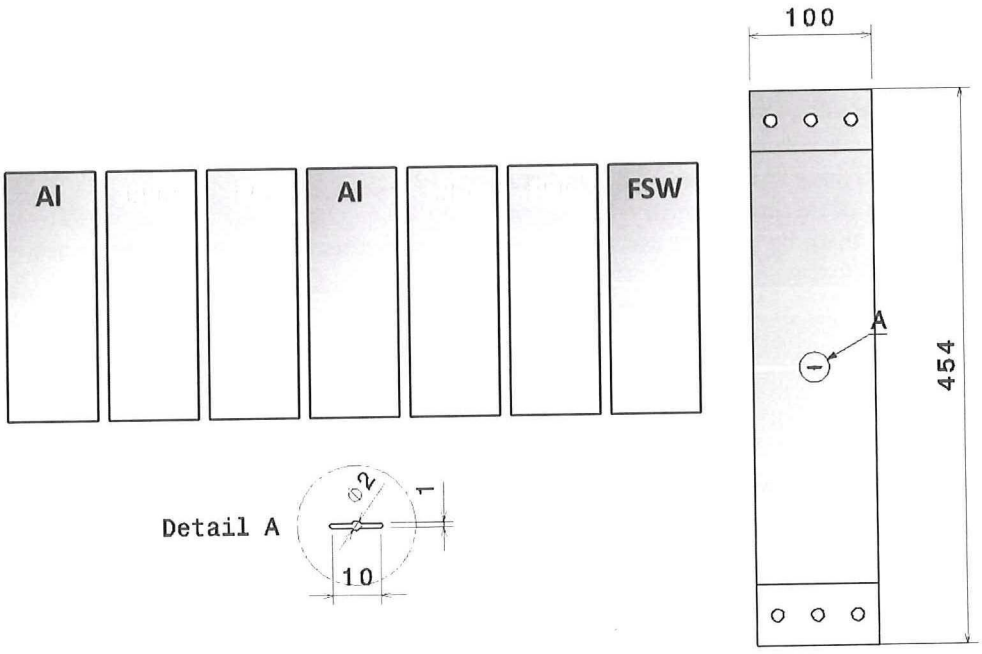

Figure 5.2: SSD crack initiation and growth test specimen (SSD1 and SSD2).

The test specimens were fatigue-loaded in a 60kN MTS test bench during which the crack size and number of load cycles were recorded. All crack initiation and growth tests were performed according to the standards set in ASTM E647 [40]. Before the real measurements were started both specimens were fatigued until a precrack of 1.4 mm had formed. Crack measurements were performed using a

USB digital camera. All of the testing parameters are summarized in table 5.1.

Table 5.1: SSD crack initiation and growth test parameters.

Specimen	Prerack stress [MPa]	Test range [MPa]	R [-]	f [Hz]
SSD1	100	100-120	0.1	10
SSD2	100	140-180	0.1	10

5.1.3 Measurements and observations

Once the experiments were performed, it was possible to measure the length of the cracks from the photos and plot the obtained values against the number of load cycles. Normally, this would be a straightforward procedure in which the length of the left and right crack are averaged and coupled to the number of load cycles. The test results for SSD1 and SSD2, however, showed that cracks in the FSW-ed layer grow significantly faster than cracks in the other metal layers. In order to show this phenomenon it was decided to not only present the measured crack growth (which is the crack growth in the FSW-ed layer), but also the expected crack length in the other layers and the newly defined 'effective' crack length.

The crack size in the other metal layers was not directly measured, but assumed to be a constant fraction of the crack size in the FSW-ed layer. These fractions were determined after the tests were performed and found to be 0.79 and 0.83 for SSD1 and SSD2 respectively. Once these numbers were known it was possible to calculate the 'effective' crack length, which is defined as the average crack length in the 3 metal layers. This effective crack length was created to allow a direct comparison of the crack growth rate in FSW-ed FMLs and standard FMLs.

Final results of the crack growth measurements are shown in figures 5.3 and 5.4 for SS1 and SSD2 respectively. In these figures, the transition point in applied stress is indicated by the black lines.

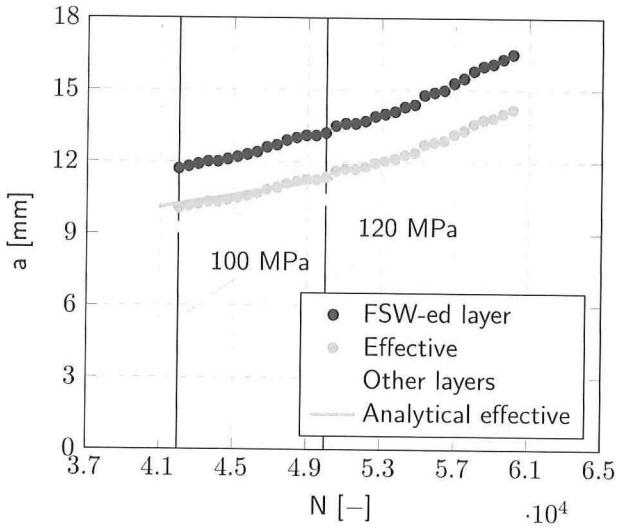

Figure 5.3: Crack size vs. number of load cycles for SSD1.

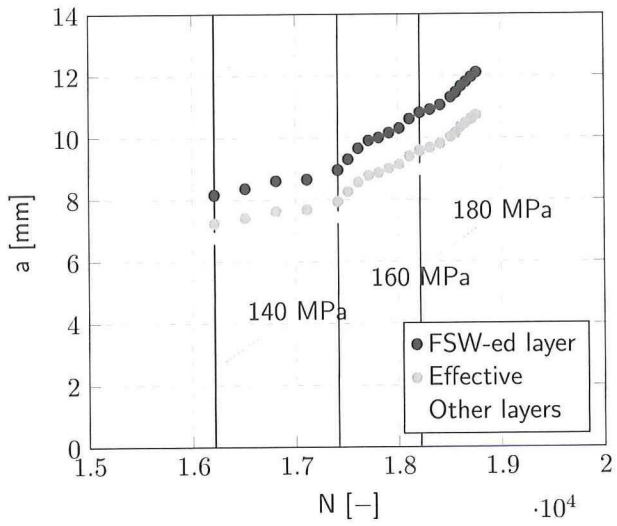

Figure 5.4: Crack size vs. number of load cycles for SSD2.

As can be seen from the figures, the effective crack length and 'other layers' crack length follow the exact same trend as the measured crack length. It is to be expected that, if the cracks in the other layers are also measured instead of assumed to be a constant fraction of the crack size in the FSW-ed layer, the trends will be different from the FSW-ed layer trend.

Concerning the morphology of the cracks, SSD2 showed the most notable behavior. Both cracks initiated from the sides of the notch in the center of the weld and continued their path there, see figure 5.5. Just before the applied stress was raised to 140 MPa, the left side of the crack traced one of the circular weld markings, which brought it in the TMAZ of the weld. There it continued to grow perpendicular to the loading direction. The right crack grew downwards at a constant angle of approximately 10° to the weld line. In the other metal layers no path deviations were observed; both crack sides grew in mode I.

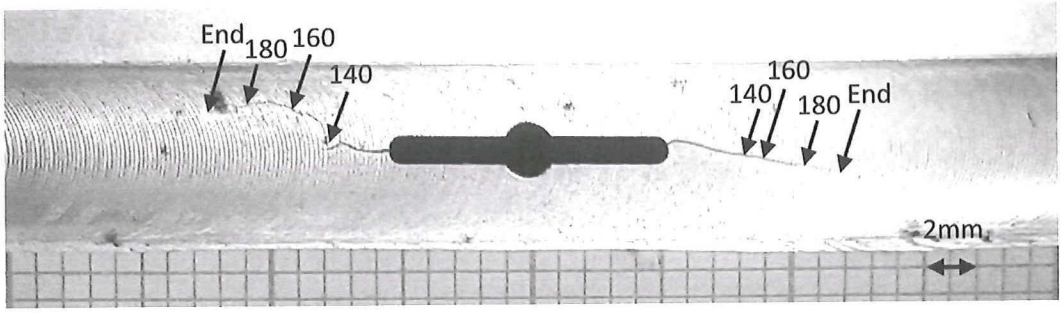

Figure 5.5: Crack morphology in SSD2 (transitions in applied stress indicated by arrows).

The cracks in SSD1 showed the same growth behavior, except for the crack that emanated from the left side of the notch in the FSW-ed layer. This crack stayed in the center of the weld throughout the whole growth period.

In both test specimens the cracks in the FSW-ed layer grew faster than the cracks in the normal

aluminum layers. To allow for a direct comparison of the growth rates in FSW-ed FMLs and standard FMLs, the effective crack length was introduced. In order to develop the required quantitative relations it was necessary to define another new variable; the effective SIF. The effective SIF is the normal SIF for a center-cracked panel where, instead of the real crack length, the effective crack length is used. Exact definitions of the 2 variables are shown as equation 5.1 and 5.2 for the effective crack length and the effective SIF respectively.

$$a_{eff} = \frac{a_{FSW} + a_{al,1} + a_{al,2}}{3} \tag{5.1}$$

$$\Delta K_{eff} = (\sigma_{max} - \sigma_{min})\sqrt{\pi a_{eff} sec(\pi \frac{a_{eff}}{W})} \tag{5.2}$$

By using these new variables in the methods set in [41], it was possible to calculate the effective crack growth rate for the FSW-ed specimens. The final results of the calculations are shown in the graph from figure 5.6. In this figure the results of the experiments (Glare 3-3/2-0.4-FSW) are marked green, reference values (standard Glare 3-3/2-0.4 from [42]) dark blue, and the results from the analytical calculations (method from Khan et al.) light blue. Note that the SIF used here is normally not used for FMLs, since it does not take fibre-bridging into account and can therefore not be used to predict the crack growth rate. The only reason for using this SIF was that it allowed the development of quantitative relations between the crack growth rates in standard Glare 3-3/2-0.4 and its FSW-ed version.

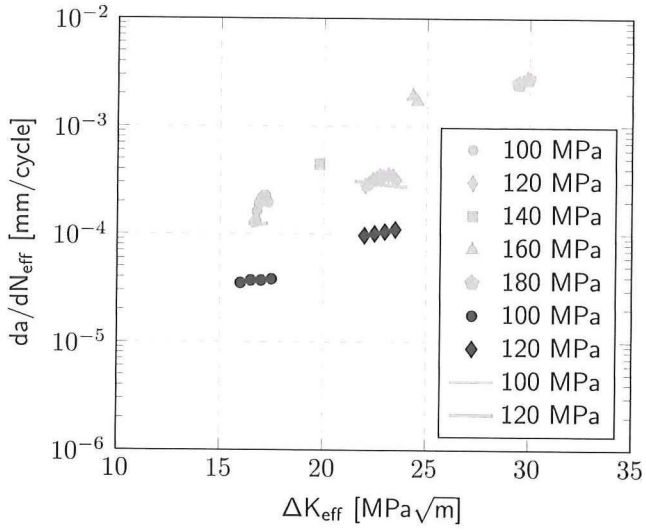

Figure 5.6: Effective crack growth rate vs. effective applied stress intensity factor at R=0.1.

Most important result from this experiment is the quantification of the difference in crack growth rate between standard Glare and FSW-ed Glare. At a maximum stress of 100 MPa, the average crack growth rate in FSW-ed Glare is 4.83 times faster than in standard Glare, whereas at a maximum stress of 120 MPa this difference decreases to 3.14 times. Since these numbers are based on very limited information, they should be used with great caution.

In addition to the quantification of the difference in crack growth rate, the experimental results were also used to check the validity of the analytical method presented in section 4.1. The three main

changes that could have been induced by the FSW-ed area were a change in modulus of elasticity, residual welding stresses, and a change in crack growth rate parameters. Ali et al. [17] showed that the Young's modulus for FSW-ed aluminum is the same as that for standard aluminum, therefore the only possible differences are an increase in crack growth rate [16, 17] and residual welding stresses. Since both of these were unknown for the used material, it was decided to implicitly incorporate them in the analysis by determining a set of collipriest variables that most accurately reproduced the crack growth. The set that produced the results from figures 5.3 and 5.6 is C1=-3.667, C2=1.90, m=0.42. Although this method does not accurately predict the crack growth rate as a function of the applied SIF, it does predict the crack growth as a function of load cycles for an applied stress of 100 MPa. The reason for only including this part of the crack growth predictions was that the model available for this research could not handle a transition in applied stress. More details on the determination of the collipriest parameters are provided in appendix A.

5.2 Multiple site damage crack initiation and growth

5.2.1 Program objective

The main objective of the MSD crack initiation and growth test program was to develop quantitative relations between the crack growth rate in standard MSD-ed Glare grades and FSW-ed Glare with MSD. Crack growth rates in MSD-ed FMLs are best measured as a function of the crack length, therefore this program was aimed at measuring this relation for the FSW-ed specimens. By relating the obtained data to already known data for standard Glare grades it is possible to develop the required quantitative relations.

5.2.2 Specimen geometry and test set-up

The specimens used in this program were of the same dimensions as the ones used in the SSD crack initiation and growth test program. One of the biggest differences compared to the SSD experiments is that in the MSD case the location of the FSW-ed aluminum sheet is varied. In the first four specimens (MSD1-4) the FSW-ed sheet is used as the center layer of the laminate, whereas in the last four specimens (MSD5-8) the FSW-ed sheet is (just as in the SSD test program) used as the outer layer. This decision was made to capture the effect of sheet location on the DT performance of the laminate. Another difference is, of course, the type of damage that was introduced in the laminate. From figure 5.7 it can be seen that three small slits were machined in the specimens to replicate the condition of MSD.

Initially, the specimens were designed to contain FSW-ed aluminum sheets with Artificial Damage (AD) at the location of the weld. This AD (which were 0.1 mm deep holes with a radius of 0.5 mm, located at the centers of the slits shown in figure 5.7) was machined into the backside of the weld to mimic the "kissing bond" (the most critical type of manufacturing damage for FSWs). These sheets were then etched, stacked into the laminate and put in the autoclave for curing. After an initial fatigue test on the MSD5 specimen, it was decided to alter the design of the specimens since the crack initiation took too long for the scope of this research. The specimens with the FSW-ed sheet as the outer layer could easily be adjusted by machining the slits in this layer. The specimens with the welded sheet as the center layer, however, required a different approach. Since the laminate was already cured at this stage, it was impossible to reach the center layer of the specimen without also machining one of the outer (non-welded) layers. This problem was solved by creating slits that went through the first two layers of the laminate, as shown in figure 5.8a.

Although this situation was not ideal, it was the only solution that still provided enough valuable information within the time-frame of this research. In order to relate the crack growth rate of the

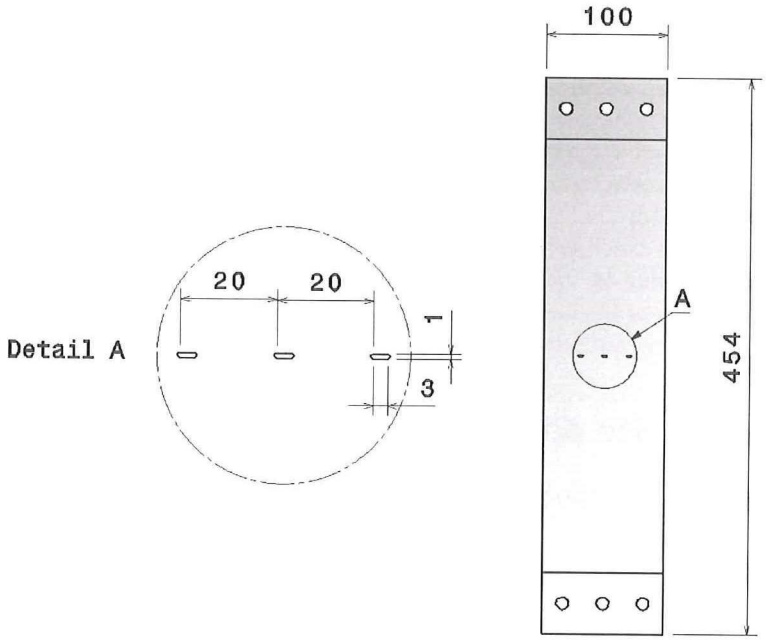

Figure 5.7: MSD crack initiation and growth test specimen (MSD1-8).

(a) MSD1-4,8

(b) MSD5-7

Figure 5.8: Cut-through of the MSD specimens at the location of the slits.

specimens with the FSW-ed layer as the center layer to the crack growth rate of the specimens with the FSW-ed layer as the outer layer, it was decided to machine one of the outer layer specimens in the same configuration as the center layer specimens. The rest of the test pieces were all of the configuration shown in figure 5.8b.

All of the specimens were fatigued in the 100 kN MTS test bench at a gross stress of 120 MPa, stress ratio of 0.05, and a frequency of 10 Hz. During the cyclic loading the crack growth was recorded using a 4MPix digital camera which was coupled to the computer to automatically relate the crack size to the number of load cycles. Since the same specimens were also used for the MSD residual strength testing program, they had to be fatigued until a different number of load cycles. The first specimen, MSD7, was fatigued until the cracks in the outer layer linked up. This condition determined how many load cycles were needed for the MSD5 and MSD6 test piece, see table 5.2. The

same procedure was followed for the rest of the specimens, but this time using the MSD8 specimen.

Table 5.2: MSD crack initiation and growth test parameters.

MSD1	MSD2	MSD3	MSD4	MSD5	MSD6	MSD7	MSD8
$1/3\ N_{fail,8}$	$2/3\ N_{fail,8}$	$N_{fail,8}$	$N_{fail,8}$	$1/3\ N_{fail,7}$	$2/3\ N_{fail,7}$	$N_{fail,7}$	$N_{fail,8}$

Two of the test pieces (MSD4 and MSD8) were torn down after the fatigue test to determine the crack growth in the non-visible layers.

5.2.3 Measurements and observations

After the experiments were performed, the crack length for each of the six locations (2 for each slit) was determined from the photos. Since the main goal of the MSD crack initiation and growth test program was to determine the crack growth in the FSW-ed layer of the specimens (without considering cracks in any of the other layers), only specimens 4, 7 and 8 were analyzed in full detail here. The measurements on MSD7 directly provided the crack size vs. the number of load cycles for FMLs with the FSW-ed layer as the outer layer, whereas the combined result of the MSD8 crack measurements and MSD4 tear down inspection could be used to predict the crack growth in FMLs with cracks in the FSW-ed center layer only. Figure 5.9 shows the final result of the crack growth measurements.

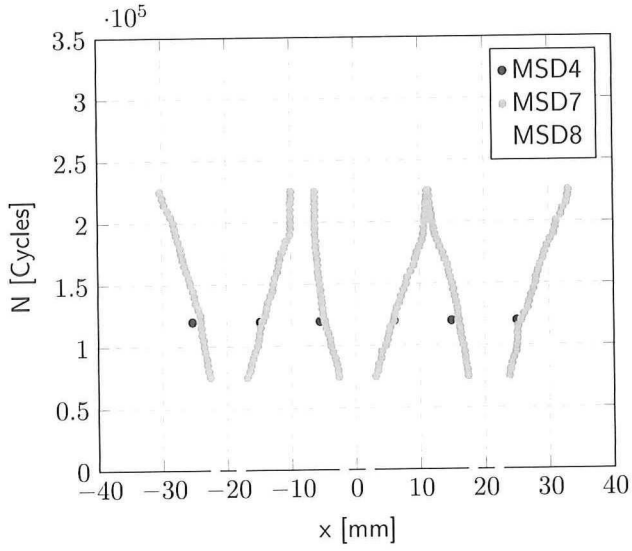

Figure 5.9: Number of load cycles vs. the crack position in the FSW-ed sheet for the MSD specimens.

From this figure it is possible to see that, after 120,000 load cycles, the cracks in the specimen with the FSW-ed sheet as the outer layer (MSD8) have grown faster than the cracks in the specimen with the welded sheet as the center layer (MSD4). (Note that only 6 data points were obtained for MSD4, because the cracks in the FSW-ed sheet could only be measured after the specimen was torn down.) By determining the average length of the cracks in both specimens and assuming that the

ratio between these numbers (of 0.476) is constant throughout the whole crack growth it is possible to predict the crack growth in specimens with the FSW-ed sheet as the center layer.

Just like the cracks in the SSD crack initiation and growth specimens, the cracks in the MSD specimens are of a mixed I-II mode. As can be seen from figure 5.10, which shows the crack morphology of MSD7, the largest part of the crack growth is perpendicular to the loading direction. Cracks that grew against the welding direction tended to move towards the TMAZ at the retreating side of the weld.

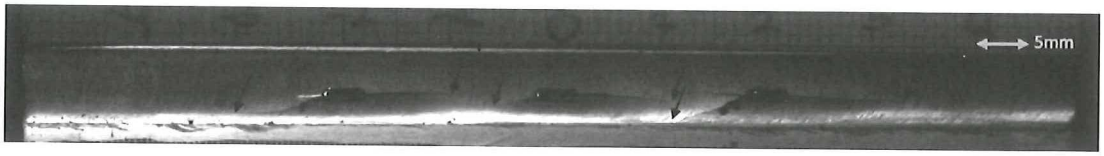

Figure 5.10: Crack morphology in MSD7 (crack ends indicated by arrows).

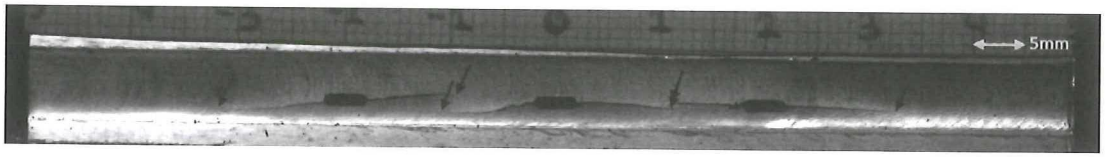

Figure 5.11: Crack morphology in MSD8 (crack ends indicated by arrows).

Similar growth patterns were observed in MSD8, see figure 5.11. In this specimen the cracks formed a more distinct 'fish-eye' pattern at link-up. An even bigger difference between the two specimen types (MSD7 with cracking in the outer layer only and MSD8 with cracks running through 2 metal and prepreg layers) was the initiation of cracks at the retreating side of the weld in MSD7. After the cracks, that initiated from the notches, showed link-up, other cracks started forming at locations where weld flash was observed. This part of the experiment was not included in the crack growth measurements from figure 5.9, but does provide valuable information for the production process. Since this kind of behavior is unwanted, it is necessary to remove the weld flash before lay-up. A more detailed view on this subject is provided in appendix A.

In both the SSD and MSD crack morphology analysis it was observed that some cracks move away from the center of the weld towards the TMAZ. This migratory behavior was not observed in the standard aluminum sheets of the laminates, suggesting that a more favorable growth path, than the center-weld path, exists in the welded sheets. In the SSD crack growth analysis it was already explained that the reason for measuring the crack growth in the center of the weld was that this is the area were the highest crack growth rates were observed [17]. Although this information is contradicted by Lemmen [19], who observed that cracks in FSW-ed Al2024-T3 grow fastest at a distance of 6 mm from the weld center-line, it is expected that it does not influence the validity of the results from the MSD crack initiation and growth test program. The MSD test program was aimed at determining crack growth rates for the 'kissing bond' defect, which is always located in the center of the weld. It is therefore safe tot say that the right notch configuration was used to obtain the crack growth.

To convert the crack length measurements to crack growth rates, the six crack lengths were averaged and, via the same method as was used in the SSD crack initiation and growth analysis, developed into average crack growth rates. These growth rates were then related to the average crack size to arrive at the results from figure 5.12.

As can be seen from this figure, cracks grow significantly faster in the specimens with the FSW-ed

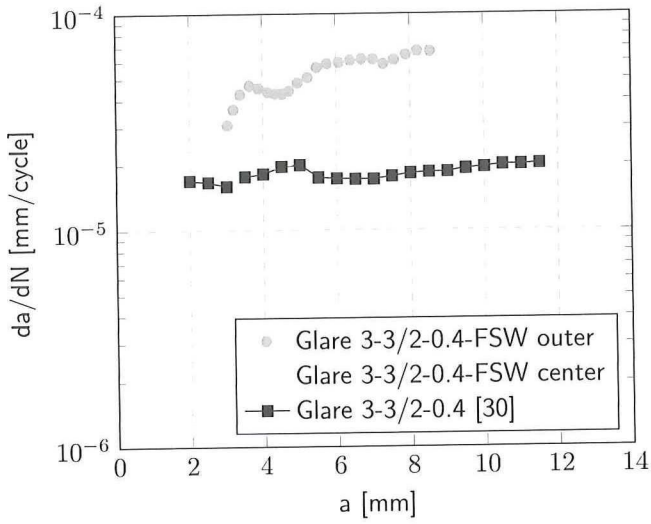

Figure 5.12: Average crack growth rate vs. the crack length for MSD specimens.

layer as the outer layer than in specimens with this layer as the center layer. After the growth rate has stabilized (which was determined as cracks larger than 5.8 mm) the average crack growth rate for Glare with the FSW-ed layer as one of the outer layers is 3.32 times the rate in standard Glare, whereas for specimens with the FSW-ed layer as the center layer this difference decreases to 1.58 times.

It should again be noted that the crack growth rate for specimens with the FSW-ed layer as the center layer was not determined directly from crack growth data since it was not possible to monitor the cracks in this layer with the applied techniques. To overcome this issue the MSD4 and MSD8 specimen were tore down, which allowed the inspection of both the outer and center layers. The average crack size in the FSW-ed layer of the MSD4 specimen (which had this layer in the center of the laminate) was subsequently determined and related to the average crack size in the FSW-ed layer of the MSD8 specimen (which had the welded sheet in the outer layer). In the data from figure 5.12 it was assumed that the crack growth rate in the FSW-ed sheet of specimens with this layer as the center layer was a constant fraction (the fraction found from the MSD4 and MSD8 tear-down inspection) of the crack growth rate for specimens with the FSW-ed sheet as the outer layer throughout the whole range of crack sizes.

5.3 Multiple site damage residual strength

5.3.1 Program objective

The purpose of the final test program, MSD residual strength, was just as the other programs to develop quantitative relations between the DT performance of standard Glare and FSW-ed Glare. For the residual strength of specimens with MSD this meant obtaining data of the residual strength vs. the amount of damage done to the specimen. A method that can be used to visualize this relationship is the damage ratio method, as presented in the chapter on DT analysis. This method presents the residual strength of the material as a function of the percentage of cracked aluminum layers. Since this information was already available from the MSD crack initiation and growth test program, the

only thing left to do was determine the residual strength of the specimens.

5.3.2 Specimen geometry and test set-up

Test specimens used in the residual strength evaluation are the ones that were not torn down for crack size inspection in the MSD crack initiation and growth test program. The two specimens that were torn down were used to determine the crack size in the non-visible layers which is information that is also necessary in the residual strength evaluation. All of the test pieces that were used in the current program are shown in table 5.3. This table shows, for each specimen, the percentage of cracked FSW layer and percentage of cracked aluminum layer.

Table 5.3: MSD residual strength test specimen geometry.

Specimen	Cracked FSW [%]	Cracked Al [%]
MSD1	12.0	8.5
MSD2	14.4	11.1
MSD3	27.9	21.5
MSD5	26.4	0.0
MSD6	91.5	0.0
MSD7	100	0.0

A standard tensile test was performed on each of these pieces to determine the force-displacement curve. The tests were done using position-control in the MTS 500 kN test bench.

5.3.3 Measurements and observations

From the force-displacement data it was possible to determine the stress-strain curve for each of the specimens. Every curve showed an initial linear elastic section, followed by plastic deformation and abrupt failure. A clear difference was visible between the specimens that had cracks in the outer layer only and the specimens with cracks in multiple layers; in the curves for the specimens with fatigue cracks in the outer layer only it was visible that the FSW-ed sheet failed far before the rest of the specimen failed. This phenomenon was not visible in the curves for the specimens with cracks in multiple layers (the specimens with the FSW-ed sheet as the center layer). More details on this subject are provided in appendix A.

In light of the residual strength evaluation, the most important data from the stress-strain curves is the maximum value of the stress. This number is the ultimate strength of the specimen and, when coupled to the crack configuration, known as the residual strength of the laminate. The residual strength of specimens 5-7 is shown in figure 5.13 as a function of the Damage Ratio (DR) in the FSW-ed layer. A value of 0 for DR_{FSW} means no cracks, and a value of 1, a fully cracked layer.

Next to the measured residual strength, the figure also shows a theoretical prediction of the residual strength of the laminate. This theoretical prediction was done using the DR method presented in section 4.4. Normally, the ultimate strength of the laminate is calculated using the material volume fraction theory, but in this case the ultimate strength was extrapolated from the measurement data and subsequently used in the DR method. The 'fitted' note in the legend therefore refers to the ultimate strength only, and not to the actual predictions. As can be seen from the figure, the resulting residual strength predictions closely match the data points. Even more important is the relation between the residual strength performance of the FSW-ed Glare and standard Glare. The

quantitative relation between the theoretical prediction and the reference material can be used to design the new concepts for FSW-ed FMLs.

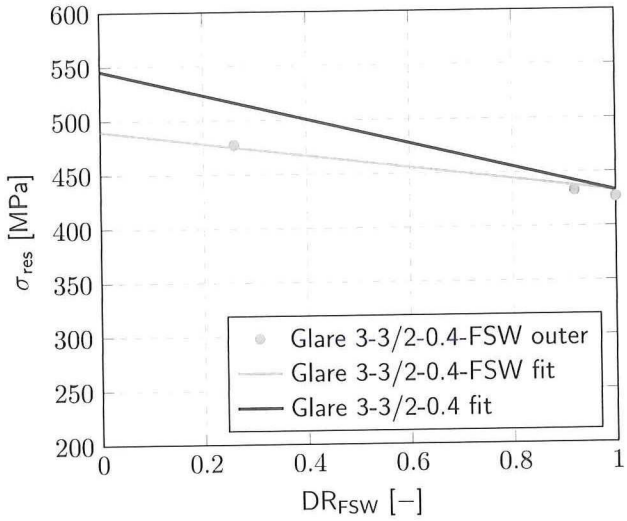

Figure 5.13: Residual strength of the laminate vs. the damage ratio in the FSW-ed sheet.

Even though the 'fitted' DR method accurately predicts the residual strength of the damaged laminates, in the current form it does not take into account the actual ultimate strength of the undamaged laminate. When looking at the difference between the 'fitted' DR method and the 'theoretical' DR method (ultimate strength calculated using the material volume fraction method) in figure 5.14, one finds that there is a gap of around 100 MPa between the two sets of predictions.

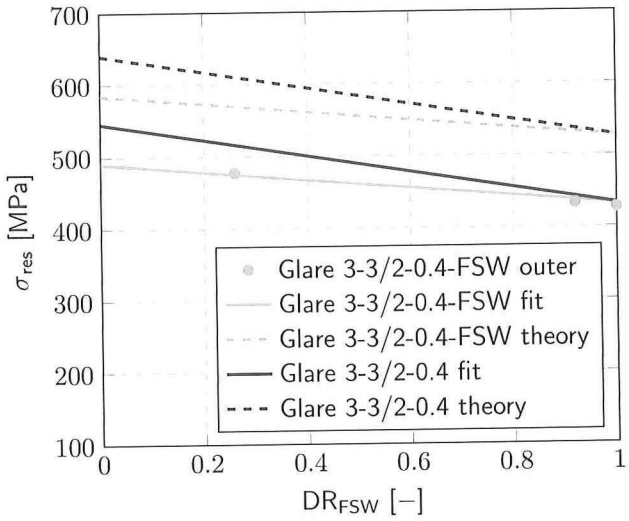

Figure 5.14: Difference between fitted residual strength and theoretical residual strength predictions.

The ultimate strength calculated with the material volume fraction method appears to be closer to realistic values than the 'fitted' ultimate strength. No reference data for Glare 3-3/2-0.4 was available, but when the ultimate strength predictions are compared to Glare 3-3/2-0.3, which has an ultimate strength of 700 MPa [43], it is possible to conclude that the material volume fraction method gives a better result. In spite of the inability to predict the ultimate strength, the 'fitted' DR method accurately predicts the residual strength of damaged FMLs. Since no anomalies were detected on the test specimen C-scans, it can be assumed that the test results are an accurate representation of reality and therefore it is possible to conclude that the 'fitted' DR method is the better method to predict the residual strength of MSD-ed FMLs. If this method is used in the lower DR-regions (DR<0.2), it will give a conservative estimation of the residual strength and will therefore, despite the prediction error, be safe to use.

A shortcoming of the method is that, in the form presented in figure 5.13, it only shows the degradation of the residual strength as a function of the DR in the FSW-ed layer. If cracking not only occurs in the FSW-ed layer, but also in one (or more) of the other aluminum layers, a 3-dimensional graph is necessary (with residual strength, DR_{al}, and DR_{FSW} on the axes, see equation 4.13) to show the effect of damage on the residual strength of the laminate. Since it is difficult to show the individual data points from table 5.3 in a 3-dimensional graph, it is useful to convert the individual DR's to the effective DR using equation 4.17. By using the effective DR it is possible to present all of the measured data in a 2-dimensional graph. The final result of this is shown in figure 5.15.

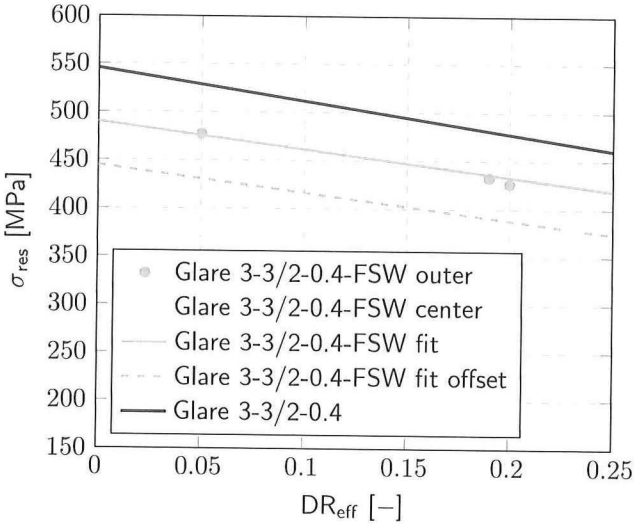

Figure 5.15: Residual strength of the laminate vs. the effective damage ratio.

Contrary to the data from the specimens with the FSW-ed sheet as one of the outer layers, the data from the specimens with the FSW-ed sheet as the center layer does not match the theoretical prediction. The difference between the theoretical prediction and the measured data for specimens 1-3 can be explained based on the configuration of the test pieces. Whereas MSD5-7 had slits in the outer FSW-ed layer only, MSD1-3 had slits running through the first 4 layers of the laminate (Al,P90,P0,FSW). Figure 5.16 shows a cut-through of the two different types of test specimens at the location of the slits. In this figure the slits are indicated by the shaded areas.

Slits in the prepreg layers reduce the residual strength of the laminate, but this reduction in residual strength is not modeled by the theory; the standard DR theory only considers damage in the

FSW-ed layer and the other metal layers. Since there is a constant gap between the measurements and the theory, it was assumed that the off-set could be modeled by a constant reduction in strength due to the cuts in the prepreg layers. The theoretical off-set prediction shown in figure 5.16 is based on the DR method, in which, on top of the cracked metal fractions, the cracked prepreg fractions were used. It should be noted that for this prediction to fit the data, it was necessary to assume that a crack of twice the total slit length was present in the prepreg layers. This suggests that it is not possible to directly use the DR method to calculate the residual strength of FMLs in which the prepreg layer is damaged. Despite this shortcoming, it can be concluded that the DR method is a feasible method to predict the residual strength of FSW-ed Glare with MSD in the metal layers.

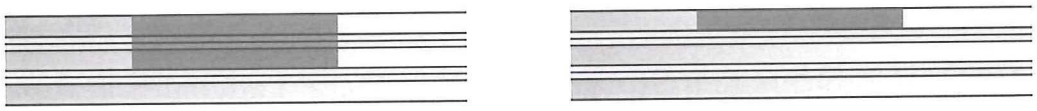

(a) MSD1-3 (FSW in center layer)

(b) MSD5-7 (FSW in outer layer)

Figure 5.16: Cut-through of the MSD specimens at the location of the slits.

Besides the validation of the analytical model, the residual strength measurements can also be used to develop a quantitative relation between the residual strength performance of standard Glare 3-3/2-0.4 and its FSW-ed version. The ratio of the two equations (the light blue line and dark blue line) shown in the figure determines how much better standard Glare performs compared to its FSW-ed version in terms of residual strength. This quantification can, together with the quantitative crack growth relations developed in earlier sections, be used to design concepts for the application of Glare with FSW-ed metal sheets in aircraft structures.

6

Application of Friction Stir Welded Fibre Metal Laminates in Aircraft Structures

In the objective of this research two project goals can be distinguished. The first goal, which was the development of DT evaluation methodologies, was already achieved in chapter 4. Although this is valuable information, it is only a small step towards achieving the final goal: the application of FMLs with FSW-ed metal sheets in aircraft structures. Before this concept can be applied in aircraft structures it is necessary to have guidelines for designing these joints. These guidelines are the second, and most important goal of the current research. This chapter will show the development of these guidelines, following the roadmap presented in chapter 3.

Since this research did not only focus on the development of design concepts, but also on the development of analytical DT evaluation methodologies, it was impossible to follow the map from the start. Instead, it was necessary to start right in the middle: relating the performance of the new structural concept to structure already verified as DT through experimental investigation. The data obtained in these experiments was used to validate the analytical methods presented earlier. These methods can now be used to develop design concepts for the application of FSW-ed FMLs in aircraft structures. Before this can be done, it is necessary to have a list of requirements for the joint. This is the subject of the first section, section 6.1. Based on these requirements and the analytical evaluation methodologies different conceptual joint designs will be presented in section 6.2. A trade-off between the different concepts is shown in section 6.3. The best concept was selected and described in more detail in section 6.4. Finally, the chapter is concluded with recommendations on which road to follow to further develop the concept of FSW-ed FMLs in section 6.5.

6.1 Requirements for the joints

The first 10 steps in the DT compliance guide (section 3.4) can all be categorized as requirements for the joint. Steps 1-3 are geometry related requirements, and steps 4-10 structural performance requirements. Since all of these requirements have to be met by the new joint design, these steps will be used as a guide to develop the list of requirements.

6.1.1 Geometrical requirements

Geometrical requirements are directly related to the location of the joint in the aircraft structure. FSW-ed FMLs are initially designed to be used as skin in fuselage panels, therefore the structural details that have to be considered in designing the joints are the ones that can typically be found in these kind of structures. A view of all structural details that can be found at the location of the joint is presented in figure 6.1.

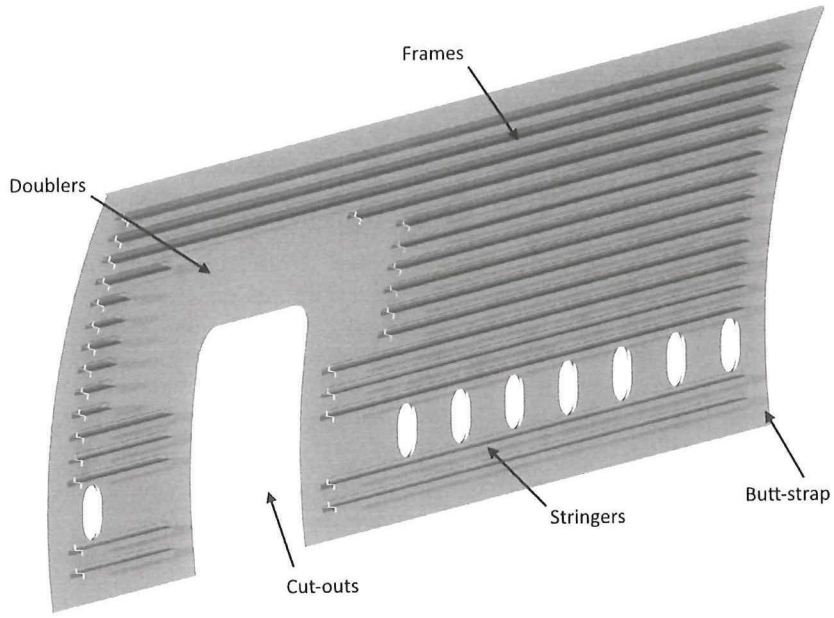

Figure 6.1: Structural details of an Airbus A380 Glare fuselage panel, (Position of currently applied splice joint indicated in orange)

Based on regulations and the structural details the following geometry related requirements can be formulated:

1. The joint shall be suitable for use at locations of significant double-curvature
2. The joint shall be flat on the inside of the fuselage panel
3. The joint shall allow for machining of cut-outs using the techniques currently applied
4. Possible locations of moisture ingress on the outside of the fuselage shall be avoided
5. The joint shall meet the accessibility provisions stated in AC 25.611

6.1.2 Structural performance requirements

The structural performance requirements cover steps 4-10 of the DT compliance guide. Among these requirements are the type of damage that has to be considered in designing the joints, the loading conditions, and the crack growth- and residual strength performance.

For the crack-growth and residual strength evaluation it is necessary to know the worst-case damage modes that can be encountered in the structure. If the joint meets the set DT performance requirements for these damage modes, all of the other damage modes are automatically also covered. Again, a distinction has to be made between the SSD scenario and the MSD scenario.

The worst-case mode for the MSD scenario was already discussed in section 2.3.3 in the literature review. In this section it was shown that the "Kissing bond" and the "Faying surface" defect are the biggest concerns when considering MSD in FSWs. Of these two, the kissing bond is the hardest to detect using the standard inspection methods. This type of processing defect is therefore considered to be the worst-case MSD mode. Zhou et al. [23] found that these defects are typically 24 μm in size, spaced at an average distance of 200 μm. Note that the defect size has been scaled to the thickness of the aluminum layers used in this research. Since the kissing bond is a defect related to the tool and material geometry, this is considered to be a valid assumption.

For the SSD scenario not only processing defects, but also service-induced defects have to be treated. The minimum size of the processing defects that can be detected in Glare is 2.2 mm [44]. Defects of a larger size are detected in the C-scan of the panels, which is performed after the panels have been cured. The size of service-induced defects that have to be examined in the DT evaluation again depends on the inspection technique used. Glare panels in the Airbus A380 require no inspection up to the LOV of the aircraft [45, 46], therefore the minimum through-crack size that has to be assumed to be present in the fuselage skin is 14.2 mm (the minimum detectable crack size for visual inspection [47]). If the same DT performance is expected for the new joint design, this is the SSD mode that has to be used in designing the concepts.

Although step 10 of the DT compliance guide is also part of the structural performance requirements it cannot be incorporated in the current evaluation since it requires the determination of the amount of damage from discrete sources. This type of damage is directly related to the design and configuration of a specific aircraft type and can therefore not be considered in the development of a general concept for the application of FMLs with FSW-ed metal sheets. The damage modes that were used in the design are summarized in table 6.1.

Table 6.1: Worst-case damage modes for the different damage scenarios.

Damage scenario	**Damage mode**	**Typical size** [mm]
SSD	Through-crack	14.2
MSD	Kissing bond	24E-3

Since the new joints are expected to perform at least as good as the splice concept (which does not require inspections up till the LOV of the aircraft) in terms of DT, the residual strength of the new design has to be equal to, or higher than, the design-limit loads at 3 times the LOV of the aircraft for both damage scenarios. The requirements concerning the structural performance can therefore be formulated as:

6. The residual strength of the joint shall be higher than, or equal to, the design-limit load at 3 times the LOV for the worst-case SSD mode

7. The residual strength of the joint shall be higher than, or equal to, the design-limit load at 3 times the LOV for the worst-case MSD mode

6.2 Conceptual design of the joint

All of the set requirements have to be met by the conceptual designs for the new type of joint. Whereas the geometrical requirements, set here, are of a more qualitative character, the structural performance requirements are fully quantitative. Before the concepts are presented, it is therefore necessary to explain the quantitative method that was used to design the different joints.

6.2.1 Design method

Since the results from the current research do not allow a variable amplitude fatigue crack initiation- and growth analysis followed by residual strength evaluation, it was necessary to design the concepts using a more simplified approach. This approach was still based on the idea that the FSW-ed joints have to perform equally well to standard Glare 3-3/2-0.4 in terms of fatigue crack growth and residual strength, but is significantly less complex.

Before the method is explained, it is useful to note that only one of the two damage scenarios had to be considered in designing the concepts. Ali et al. [17] investigated the crack formation originating from defects and oxide inclusions in FSW-ed Al2024-T351. In their research it was shown that, with the FSW in the as-welded condition, no cracks originated from defects of 50 μm in size at stress ranges below 150 MPa (R=0.1). The upper limit on the size range of the kissing bond defect was found to be 24 μm. This implies that no cracks will originate from these types of defects at the typical stress range of 108 MPa (R=0.1) found in fuselage skins, and MSD does not have to be considered in designing the joints.

As a result, the crack growth analysis is fully focused on SSD. In the SSD test program it was found that the crack growth rate in the FSW-ed laminate is 3.14 times the crack growth rate in the standard laminate, at an applied gross stress of 120 MPa. To lower the crack growth rate in FSW-ed Glare (at 120 MPa applied stress) to the level found in standard Glare 3-3/2-0.4, it is necessary to reduce the stress in the metal layers to the level at 100 MPa applied stress, see figure 5.6. This can be done by adding extra layers of aluminum or prepreg at the location of the welds until the desired stress level is reached. The stresses in the metal layers had to be decreased from 137.7 MPa (120 MPa applied) to below 112.9 MPa (100 MPa applied).

Finally, the joint had to be designed for residual strength. This would normally be done by determining the design limit loads, and designing the joint to have sufficient residual strength after it has been fatigued up to the required number of load cycles. Since the fatigue information is not available in the current analysis, it was decided to use an alternative method. The residual strength of the FSW-ed laminate has to be equal to, or larger than, the residual strength of the standard laminate over the whole DR-range. In other words; the line for the residual strength of the FSW-ed concept has to be higher than the line for Glare 3-3/2-0.4 in figure 5.15.

The structural performance requirements described in this section were, together with the geometrical requirements, used to design 4 different concepts for the application of FMLs (in this case Glare 3-3/2-0.4) with FSW-ed metal sheets in aircraft structures. Each of the concepts will be described in detail in the following sections.

6.2.2 Concept 1 - Inter-laminar doubler

The first concept that meets both the geometrical and structural performance requirements, is a laminate with an inter-laminar doubler of 0.4 mm thick. A cut-trough of this concept is shown in figure 6.2. As can be seen from subfigure a, the transition from the base laminate to the FSW-ed part requires only one thickness step in the outer 90° prepreg layer and the outer aluminum layer. At the locations of the welds the laminate is build up from 4 aluminum layers of 0.4 mm thick, plus the prepreg layers, already present in the standard laminate.

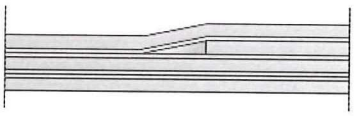

(a) Transition from standard laminate to FSW-ed part

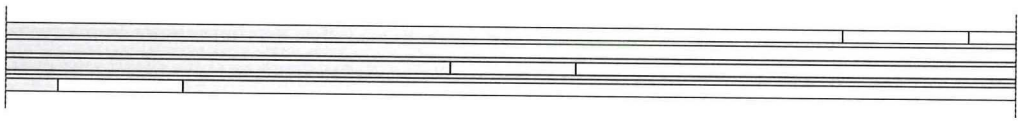

(b) Part of the joint with the FSW-ed areas

Figure 6.2: Cross-sectional view of the first concept.

The FSWs are interspaced at a distance of 38 mm (1.5 inch), measured from the centerlines of the welds. This means that the inter-laminar doubler needs to have a total width of 173 mm. A summary of the laminate lay-up is provided in table 6.2.

Table 6.2: Laminate lay-up at the location of the weld for concept 1.

Layer	**Thickness** [mm]	**Width** [mm]
Al2024-T3	0.4	-
FM94 prepreg 90°	0.133	-
Al2024-T3	0.4	173
FM94 prepreg 0°	0.133	-
Al2024-T3	0.4	-
FM94 prepreg 0°	0.133	-
FM94 prepreg 90°	0.133	-
Al2024-T3	0.4	-

As a consequence of the added aluminum layer, the stress in the metal layers at the location of the welds has dropped to a value of 107.3 MPa (applied stress of 120 MPa on the standard laminate). This value is below the limit of 112.9 MPa, which is shown as the green line in figure 6.5. Furthermore has the residual strength rate (defined as the fraction of ultimate strength over the load on the laminate at an applied stress of 120 MPa on the standard laminate) increased to a level above that of standard Glare 3-3/2-0.4, over the complete DR-range. The residual strength rate of the different concepts is shown in figure 6.6.

6.2.3 Concept 2 - Extra prepreg layers

The second concept is a laminate that has extra prepreg layers at the location of the welds. As can be seen from figure 6.3, 3 prepreg layers are added underneath the outer aluminum layer. One of these layers is longer than the other two, to decrease the thickness steps involved and thus lower the stress concentrations.

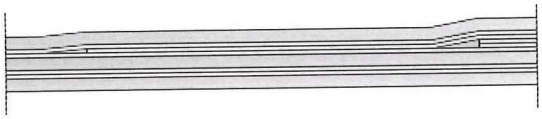

(a) Transition from standard laminate to FSW-ed part

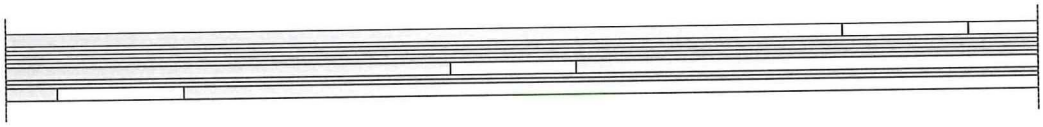

(b) Part of the joint with the FSW-ed areas

Figure 6.3: Cross-sectional view of the second concept.

All of the added prepreg layers are of the 90°-type, since these are most effective in lowering the stresses in the aluminum layers, and increasing the ultimate strength of the laminate. A complete description of the laminate is given in table 6.3.

Table 6.3: Laminate lay-up at the location of the weld for concept 2.

Layer	**Thickness** [mm]	**Width** [mm]
Al2024-T3	0.4	-
FM94 prepreg 90°	0.133	-
FM94 prepreg 90°	0.133	290
FM94 prepreg 90°	0.133	173
FM94 prepreg 90°	0.133	173
FM94 prepreg 0°	0.133	-
Al2024-T3	0.4	-
FM94 prepreg 0°	0.133	-
FM94 prepreg 90°	0.133	-
Al2024-T3	0.4	-

As can be seen from figures 6.5 and 6.6, both the crack growth rate, and residual strength requirements are met by the concept. Interesting to note, however, is the difference between concept 2a (the concept presented in this section) and concept 2b (the same concept, with only 2 added prepreg layers). The stress level in the metal layers gets close to the required limit. Supported by the fact that the residual strength of this material is still higher than that of standard Glare 3-3/2-0.4, it might be possible that 2 extra prepreg layers is enough. At this moment, there is not enough information to support this claim and therefore only concept 2a will be considered as an option.

6.2.4 Concept 3 - Inter-laminar doubler + extra prepreg layer

The third concept is a combination of the first two concepts; an inter-laminar doubler supported by an extra prepreg layer. In stead of the 0.4 mm thick doubler from the first concept, this concept uses a doubler of 0.3 mm in thickness. The complete configuration is summarized in figure 6.4 and table 6.4.

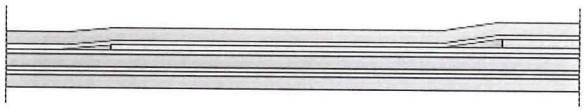

(a) Transition from standard laminate to FSW-ed part

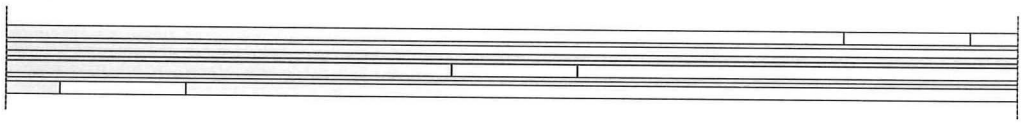

(b) Part of the joint with the FSW-ed areas

Figure 6.4: Cross-sectional view of the third concept.

Table 6.4: Laminate lay-up at the location of the weld for concept 3.

Layer	**Thickness** [mm]	**Width** [mm]
Al2024-T3	0.4	-
FM94 prepreg 90°	0.133	-
Al2024-T3	0.3	173
FM94 prepreg 90°	0.133	290
FM94 prepreg 0°	0.133	-
Al2024-T3	0.4	-
FM94 prepreg 0°	0.133	-
FM94 prepreg 90°	0.133	-
Al2024-T3	0.4	-

6.2.5 Concept 4 - Laser peening

The final concept, concept 4, is completely different from the other three concepts. Instead of adding material at the location of the welds, the required decrease in crack growth rate and increase in residual strength, is achieved by introducing compressive residual stresses in the welds.

Hatamleh et al. [48] investigated the influence of laser peening on the crack growth rate and tensile properties of FSW-ed Al7075-T7351. This research showed that, under the right conditions, crack growth rates in the weld equal to, or lower than, that in the base material are achievable using this method. Since the aluminum used in the current research is of a different grade, it is not possible to use the data from their research. It is, however, interesting to see (under the assumption that the

crack growth rate and residual strength requirements can be met by laser peening the welds only) how this concept performs compared to the other three concepts.

6.2.6 Structural performance

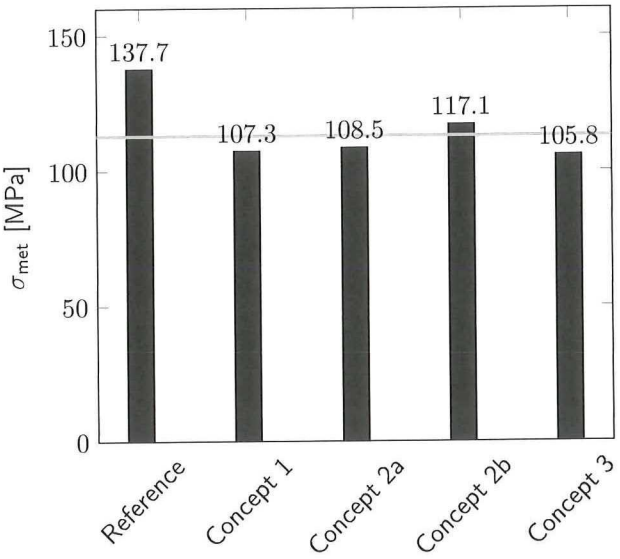

Figure 6.5: Stress in the metal layers of the different concepts, at 120 MPa applied stress.

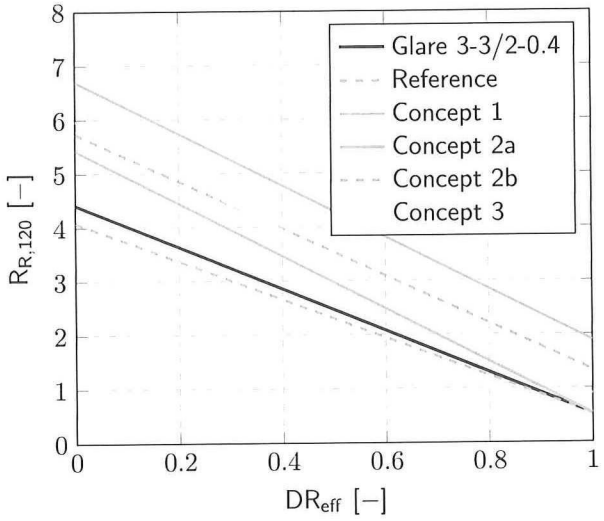

Figure 6.6: Residual strength rate at an applied stress of 120 MPa vs. the effective damage ratio.

6.3 Selecting the best concept

The question now is: Which of these concepts is the best? Or, to be more specific: Which concept provides the optimum 'value'? In order to answer this last question it is necessary to define 'value' using the idea of value analysis. Based on the resulting definition it is possible to rank the different concepts and select the best one.

6.3.1 The idea of value analysis

Selecting the best performing design from a list of concepts is a process that ideally considers multiple aspects of the design at the same time. By expressing the different performance parameters all in the same units it is possible to rank the ideas. The concept with the highest value, resulting from the analysis, is considered to be the best.

This method, called value-analysis, applied to aerospace projects used to have as goal to make everything "better, cheaper, and faster" [49]. Recently, this has shifted to: "more affordable, cleaner and quieter". The value of a design can therefore be expressed as [50]:

$$value = \frac{1}{f_{lcc} f_n f_e} \tag{6.1}$$

In this equation f_{lcc} is a function of the life-cycle costs, f_n a function of the noise, and f_e a function of the emissions. By determining these functions for FMLs with FSW-ed metal sheets and evaluating the different concepts, it is possible to select the best performing idea. The concept with the highest value ultimately wins the face-off.

6.3.2 Value analysis applied to FSW-ed FMLs

While all of the functions in equation 6.1 are important when designing an aircraft engine for example, not all of them are fully applicable when considering the concept of FSW-ed FMLs. The noise function in this case is of little importance since a change in fuselage joint design will not significantly affect the noise performance of the aircraft. It is therefore assumed that this function can be dropped in the current analysis.

The emission function is the sum of operating emissions and manufacturing emissions. If it is assumed that the difference in manufacturing emissions between the different concepts is negligible (which is a reasonable assumption considering the small differences in design between the concepts), only the operating emissions are left. Operating emissions are mainly affected by the weight of the aircraft (higher weight leads to more fuel consumption, which again leads to higher emissions). Although this is given as a separate function in the equation for the value, it can be incorporated in the function for the life-cycle costs since manufacturing emissions are of no influence here. The operating emissions can be expressed in monetary values by determining the amount of emissions released into the atmosphere as a function of the increase in aircraft weight and relating this number to the accepted cost of emission capture.

As a result, the 'value' is a function of the life-cycle costs only. This function can further be subdivided in manufacturing, operating, service, maintenance, repair and disposal cost. The biggest differences between the concepts will be found in the Direct Operating Cost (DOC). DOC covers the manufacturing costs and operating cost [51], see equation 6.2.

$$DOC = C_{man} + pM_s \tag{6.2}$$

In this equation C_{man} are the manufacturing costs, p a life-time fuel cost factor which can be found in [52], and M_s the mass of the structure.

At this point it is interesting to not only look at the difference in value between the different concepts, but also compare their performance to that of the splice concept. By using standard Glare 3 as a reference point, it is possible to only consider the increase in mass and manufacturing costs, which reduces the computation time without influencing the final results. The variable of interest thus becomes ΔDOC; the difference between the DOC of the concept and the DOC of standard Glare 3. To keep things comparable all $\Delta DOCs$ are calculated per unit length. Combining all of the foregoing, results in the following equation for the value:

$$value = \frac{1}{\Delta DOC} \tag{6.3}$$

6.3.3 Value of the different concepts

After all of the calculation steps (details are presented in appendix B) were performed, the results from table 6.5 were obtained. This table shows the final value of the concepts, both in- and excluding the material costs. The reason for including both of these values was that no exact numbers were available for the material costs.

Table 6.5: Value of the different design concepts.

Concept	**Value** Excl. [mm/€]	**Value** Incl. [mm/€]
Splice	603.9	26.6
FSW-ed Glare	133.3	133.3
Concept 1	25.8	1.86
Concept 2	50.5	1.59
Concept 3	27.4	1.45
Concept 4	0.04	0.04

From the results in the table it is clear that concept 2 gives the highest value if material cost is not considered. This situation changes if these costs are incorporated in the analysis; instead of concept 2, concept 1 comes out as the best design. It needs to be noted, however, that the values shown in table 6.5 were calculated for the situation in which the cost per unit volume for Al2024-T3 is equal to the cost per unit volume for FM94 prepreg. If the cost of FM94 prepreg drops to 84% of the cost of the aluminum, concept 2 becomes the best performing idea again. Since it is not expected that the cost of prepreg becomes this much lower than the cost of aluminum, it is safe to say that concept 1 is the best design.

Even though this design comes out as the best, its value is still significantly below that of the spliced version of the laminate. The only thing that is not incorporated in the numbers from the table is the amount of labour involved in the lay-up process. Although it is to be expected that it takes more time to lay up the splices, it does not close the difference in value between the two designs. Even if it takes 10 times longer to lay-up the spliced laminate, the value of it remains higher than that of concept 1.

6.4 Critical review of the selected concept

Based on this fact, it is already possible to conclude that the concept of FMLs with FSW-ed sheets is no viable alternative to the splice concept. The only aspect in which splicing performs less, is the

applicability of the joint at locations where significant double curvatures are required. FSW-ed FMLs can, in contrast to spliced laminates, be applied at these locations.

In order to see whether this is a realistic option, the concept has to be compared to other materials typically applied in aircraft structures. Given the time and information available, the best method to do this is to look at two material properties that are used to determine the DT-performance; the specific fracture toughness and the specific ultimate strength. Higher values for both of these properties, indicate a better performance. Materials that are located towards the top right corner of figure 6.7, therefore are considered to be more suitable alternatives when designing for DT.

The figure shows the range in specific fracture toughness and ultimate strength for aluminum alloys, Glass Fibre Reinforced Polymers (GFRP), and Carbon Fibre Reinforced Polymers (CFRP) [53]. To show the effect of the FSW-ed region (concept 1) on the performance of the laminate, both the point for standard Glare 3-3/2-0.4, and the point for the FSW-ed concept version are included in the graph. Due to a lack of information, the fracture toughness of the standard laminate had to be assumed to be equal to the fracture toughness of Glare 3-3/2-0.3 from [39]. The DT-performance values for the FSW-ed concept were assumed to be equal to those of the standard laminate, adjusted for the difference in density. Depending on the spacing of the joints the density is calculated as a weighted volume fraction. The point in the graph is for the case where the spacing is equal to the joint width (the limit case).

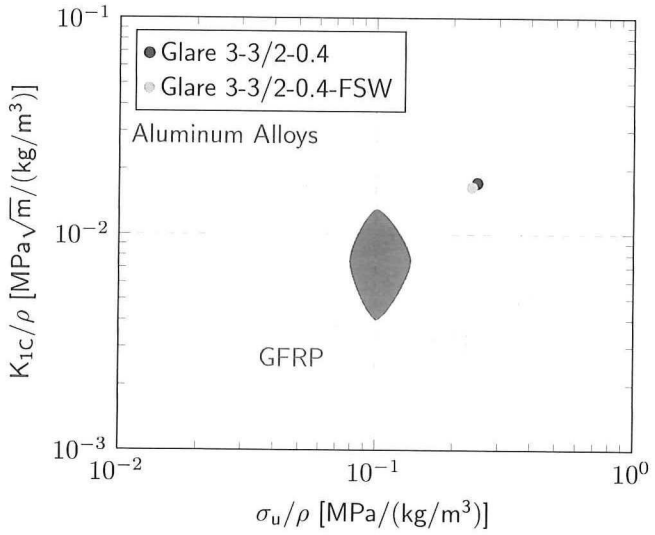

Figure 6.7: Specific fracture toughness vs. specific ultimate strength for different materials.

As can be seen from the graph, the DT performance of the FSW-ed concept is close to the DT performance of the standard laminate, even for the case where all of the laminate has 4 layers of aluminum. Next to this, the concept also scores better than all of the aluminum alloys, all of the GFRPs and a large part of the CFRPs. The only materials that have more favorable DT properties are the CFRPs towards the top right corner of the graph.

Although the analysis is based on limited experimental data, it is possible to draw some general conclusions already. First of these is that Glare with FSW-ed metal sheets cannot compete with spliced Glare in terms of cost effectiveness. Only if the structure has significant double curvatures, and Glare is considered to be the best material, the FSW-ed concept should be chosen. When looking at other materials, the concept has better DT characteristics than all of the aluminum alloys and all

of the GFRPs, but scores lower than some CFRPs. It should be noted that the comparison with other materials is based on only two material properties and should therefore be treated with great caution. When looking at cost (which is a major design driver), the ranking of the materials may be different.

6.5 Towards the application of FSW-ed FMLs in aircraft structures

The selection of the material for the specific parts where double curvatures are required, depends on the outcome of a cost estimation. Before anything is done, it is therefore necessary to look at the cost-effectiveness of FSW-ed Glare compared to CFRPs. Only if the newly developed concept turns out to be the best design, a more detailed analytic and experimental program need to be carried out.

The research presented in this paper was focused on determining the effect of the FSW-ed metal sheets on the DT performance of the laminate. In the experimental program, the crack growth and residual strength characteristics of the FSW-ed version of Glare 3-3/2-0.4 were measured. The obtained results were related to the DT characteristics of the standard laminate, which provided the information necessary to develop a concept for the application of FSW-ed FMLs in aircraft structures. When looking at the roadmap presented in section 3.4, it is clear that, before the concept can be applied in aircraft structures, it is essential to analytically and experimentally prove that the concept meets the set requirements.

Even though it is possible to follow the list from the start, it might be better to first check whether the selected concept performs as expected. A relatively simple, yet sufficiently accurate, test will be to determine the crack growth rate as a function of the SIF in the newly developed concept at 120 MPa applied stress on the standard laminate. The test piece should have the laminate with the internal doubler as the upper half and the standard laminate as the lower half, to allow accurate comparison of the crack growth rates. If the crack growth rate in the new concept is equal to, or lower than, that in the standard laminate, it is safe to say that the design meets the initial crack growth requirement. Both halves of the laminate should subsequently be tested for residual strength (at the same crack length), to see whether the residual strength requirement is also met.

In addition to these tests, it is advisable to determine the SSD residual strength performance of the FSW-ed version of Glare 3-3/2-0.4. The experimental program carried out in this research only considered the SSD and MSD crack initiation and growth, and MSD residual strength of the laminate. Due to problems with the measurement equipment, it was not possible to determine the K_R-curve for Glare 3-3/2-0.4-FSW, which was necessary to quantify the difference in SSD residual strength performance between the standard laminate and its FSW-ed version. The measured K_R-curve should be used to develop a trend that relates the residual strength to the crack size, using the methods set in chapter 4. By doing the same for standard Glare 3-3/2-0.4, it is possible to quantify the difference in residual strength performance between the two types of laminates. This quantification can subsequently be used to check whether the designed concept also meets the SSD residual strength requirement. Even though the K_R-curve method cannot be used for fatigue cracks, it does give a good indication of the influence of the FSW-ed areas on the residual strength performance of the laminate. To put the results in the right perspective, the quantified difference for the SSD case can be compared to the MSD case; similar differences indicate that the K_R-curve method is a valid approach to proving SSD residual strength characteristics.

If all requirements are met, it is possible to continue with the next step: the crack initiation analysis. One of the benefits of (FSW-ed) FMLs compared to, for example, standard metals is that they are considered to be a multiple load-path structure. A multiple load-path structure is a structure in which, if one the load-paths fails, the load will be redistributed over the other, remaining, paths. Or, applied to FMLs, if one the layers fails, the other layers will carry the redistributed load. In

a single load path material, failure of one layer (the only layer), results in failure of the complete structure. The difference between a typical single load-path material and a typical multiple load-path material is shown in figure 6.8. In this figure the failed regions are indicated by the shaded areas.

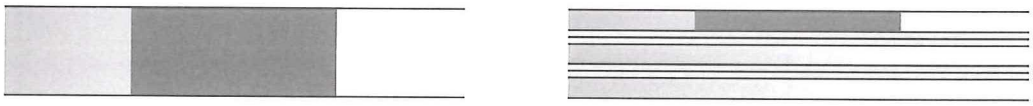

(a) Standard metal (single load path) (b) (FSW-ed) FML (multiple load path)

Figure 6.8: Difference between single- and multiple load path materials.

Although both types of materials can be used in DT structures, they require a different design approach. Single load-path structures are designed based on the slow crack growth method, whereas multiple load-path structures are designed fail safe. The difference between these two methods is shown in figure 6.9. In fail safe design, the Crack Growth Life (CGL) is defined as the period from detectable crack size in one of the elements to critical crack size in the complete structure. In slow crack growth design this period is defined as the time from detectable crack size in the only element to critical crack size in the same element.

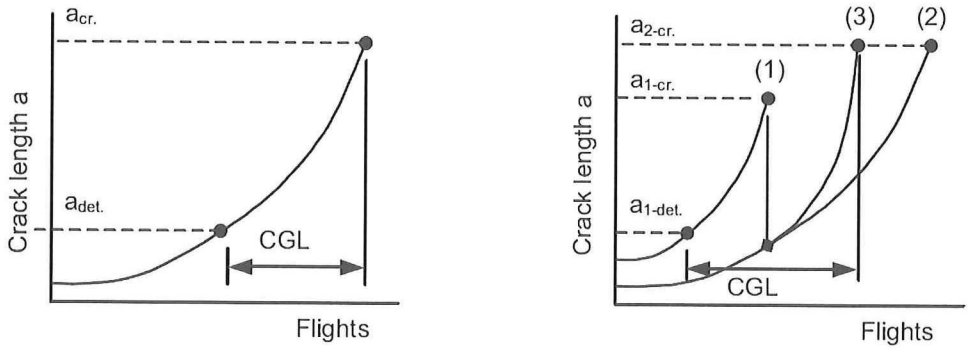

(a) Single load path structure (b) Multiple load path structure

Figure 6.9: Damage tolerant design approach [32].

An important aspect of fail safe design is that it is possible to benefit from crack initiation atop of crack propagation. In standard FMLs and spliced FMLs, the combination of crack initiation and crack propagation time ensures an inspection-free structure. Crack propagation and residual strength (both at, or above, the performance level of the standard FML) were already considered in the design of the concepts for FSW-ed FMLs, but in order to ensure an inspection-free structure it has to be shown that the crack initiation period is the same as, or better than, that of the standard laminate.

In the crack initiation analysis it is necessary to look at the maximum allowable defect size, given the expected stress level; no crack initiation may occur from processing defects at operational stress levels. The post-weld inspection program should ensure that welds with defects larger than the

maximum allowable size do not pass the inspection. Ali et al. [17] observed that no cracks initiated from defects of 50 μm in size at an applied stress range of 150 MPa. Since it is expected that the maximum operational stress range in the metal layers will be around 120 MPa, it can be concluded that, if the maximum allowable defect size during the ultrasonic phased array scanning is set to 50 μm, no crack initiation will occur in the FSW-ed layers. The only type of defect that cannot be detected using ultrasonic phased array or visual inspection is the 'kissing bond'. This defect, however, has a maximum size of 24 μm, which is smaller than the maximum allowable defect size.

Regardless of these observations it will be necessary to perform a more in-depth crack initiation analysis. The main drivers in this analysis will be the reliability and feasibility of the weld inspection program. By setting the maximum defect size at 50 μm, it is theoretically possible (under the assumption that the maximum stress range in the FSW-ed layers will be lower than 150 MPa) to avoid crack initiation in the FSW-ed layers . Before this method can be applied it is necessary to validate this theory and check the cost-effectiveness of the complete production- and inspection process (as part of the detailed cost-effectiveness analysis of FSW-ed FMLs in general). The validation of the 'no crack-initiation'-theory can be done by inspecting FSW-ed samples for defects using the proposed inspection method, and subsequently test the samples at the maximum applied stress range to see whether crack initiation occurs or not. If crack initiation is not observed, it is possible to conclude that, for this specific combination of production, inspection, and concept design, no in-service inspections are required. Moreover, if it is shown that crack initiation does not occur in the welded region, it is possible to view FSW-ed FMLs as a standard material and not as a joint, meaning no joint-specific compliance requirements have to be met.

If it cannot be shown that the welded region is free from crack initiation, it is necessary to view the material as a joint. Under these conditions the DT compliance plan has to be followed. To begin with, the exact location of the joint in the aircraft structure has to be determined. This is necessary to find the design-limit loads, DSG, LOV, and loading conditions for the joint. For all of the three damage situations (SSD, MSD (this situation only has to be considered if it is expected that a large portion of the load spectrum results in stress ranges of 150 MPa or higher in the FSW-ed sheet of the laminate), and DSD) the DT performance has to be calculated analytically. The necessary tools to do this were presented in chapter 4. Before the SSD model can be used, the residual stresses in- and Paris constants for- the welded region need to be determined experimentally. If these values are known, it is possible (after validation of the model) to determine the crack growth rate using the method. The residual strength model presented here provides good results for situations in which the prepreg layers are fully intact, but does not allow for residual strength predictions in situations with through-cracks. A different model is required to analytically calculate the required values for this situation.

When the designed concept meets the set requirements, testing is needed to support the findings. These tests can either be full-scale (for a complete new aircraft), or on coupons (for type design changes). The latter option allows for relating the performance of the new concept to that of the standard laminate. By using test pieces that have the FSW-concept as the upper part, and the standard laminate as the lower part it is possible to relate the DT performance of both laminates directly (it needs to be noted that weld flash has to be removed before lay-up, to prevent crack initiation at these locations). The resulting quantitative relations for the crack growth rate and residual strength can then be used to design the complete structure. Finally, the LOV (and possible maintenance and inspection tasks if the requirements for the design are relaxed) have to be included in the ALS of the aircraft.

When all of the aforementioned checks, analyses, tests, and design tasks have been performed, the concept of FMLs with FSW-ed metal sheets is finally ready to be applied in aircraft structures.

7

Conclusions and Recommendations

In the current generation of aircraft, FMLs are mainly applied as skin material in the fuselage. At these specific locations, large FML sheets are necessary. This directly led to one of the biggest design challenges faced in the development of FMLs; due to limitations on the maximum width of thin metal sheets, it was necessary to develop a method for joining FML panels. After multiple attempts to find a solution that met all the requirements, the splice technique was discovered. This technique makes use of overlapping metal sheets at the location of the joint to reach the required DT performance. Although this method is successfully applied in aircraft structures, it has one significant limitation: due to the complexity of the joint it cannot be applied at locations where significant double curvatures are required. A method that overcomes this problem is the concept of FSW-ed FMLs; the thin metal sheets are welded together before lay-up, making it possible to create double curved structures. Before this idea can be applied in aircraft structures, it is necessary to certify it as DT. The DT performance of FSW-ed metal sheets was already known from work by other researchers, but the characteristics of the material in the form of a FML were still undiscovered. To certify a structure or material as DT, it has to be shown, using both analytic and experimental methods, that it meets the set requirements. The goal of this research was to make recommendation to Airbus on the DT certification of FMLs with FSW-ed metal sheets, by identifying the required DT evaluation methodologies and establishing design guidelines for these types of joints.

In order to reach this goal, multiple steps were taken. First, literature was consulted to identify the starting point of the research and to determine the DT characteristics of FSW-ed metal sheets. Before anything was done with this information, a DT certification plan was constructed based on the method from the FAA. This step-by-step guide was used as the roadmap for the final development of the design guidelines for FSW-ed FMLs. The first necessities identified in this plan were analytical methods for determining the crack growth rate and residual strength of the laminates with FSW-ed sheets. Proven methods for analyzing these characteristics for standard FMLs were identified and advise was given on how to incorporate the effect of the FSW-ed areas in the models. The second step in the plan was the development of quantitative relations between the DT characteristics of a standard laminate and its FSW-ed version. Crack growth rates and residual strength of Glare 3-3/2-0.4-FSW were determined and related to the performance of Glare 3-3/2-0.4, to come up with the required relations. These quantitative relations were subsequently used to develop different concepts that had, at a minimum, the same DT characteristics as the standard laminate. Out of the designed concepts, the most cost-effective one was chosen for further analysis. The DT performance of the

new concept was compared to other typical aerospace materials, and recommendations were made on which steps to follow before FSW-ed FMLs can be applied in aircraft structures.

Concerning the analytical methods for determining the DT performance of the new laminate type, it is expected that the conventional crack initiation and growth methods can be used to predict the crack growth rate in the FSW-ed metal sheets, if the residual welding stresses are added to the total stress level in the metal layer and the right crack growth parameters are used. A relatively simple method, the DR-method, was used to predict the residual strength of the fractured laminates. The application of this model is limited to cases in which the prepreg layers are intact and can therefore not be used for through cracks. A residual strength prediction model that can handle combinations of SSD, MSD, through cracks, and part-through cracks is not available at this moment.

The experimental results pointed out that SSD through cracks in the center of the weld grow, at a maximum, 4.83 times faster in FSW-ed Glare than SSD through cracks in standard Glare. It was observed that cracks in the FSW-ed aluminum layer grew faster than the cracks in the normal aluminum layers. To determine the difference in crack growth rate between the standard laminate and the FSW-ed laminate, the effective crack length (average crack length over the 3 layers) was used. Since MSD can occur in FSWs due to the typical repetitive flaws that can be introduced in the weld during the production process, it was necessary to determine the crack growth rates for this damage mode as well. The results from these tests showed that cracks grow, on average, 3.32 times faster in FSW-ed Glare 3-3/2-0.4 than in the standard version of the laminate. A difference in crack growth was observed between the outer and the inner layer of the laminate; in the outer layer cracks grew significantly faster. If stress ranges in the FSW-ed layers stay below 150 MPa, no crack initiation will occur from root flaws, and MSD is not considered to be the leading design factor. Like the crack growth performance, the residual strength performance of FSW-ed laminates was also lower than that of the standard laminates. From the measurements it was possible to see that the residual strength was lower for all of the damage ratios (fraction of cracked aluminum over initial pristine aluminum) considered. It should be noted that the residual strength evaluation was limited to cases where all prepreg layers were intact, meaning that through cracks were not analyzed.

Despite this limitation, the experimental results were used to design four concepts that brought the DT-performance of the FSW-ed version of Glare 3-3/2-0.4 back to the performance level of the standard laminate. Out of these four concepts, the concept with the internal Al2024-T3 doubler of 0.4 mm thick was found to be the most cost-effective option. The results from the cost-analysis also clearly showed that FSW-ing cannot compete with splicing as a method for joining FML panels in terms of cost-effectiveness. As a result, the concept should only be applied at locations where splicing is not an option. Compared to other typical aerospace materials, the new idea performs better than GFRPs and aluminum alloys in terms of DT, but scores lower than some CFRPs.

Before the material can be applied in aircraft structures, it is therefore advisable to check how cost-effective FSW-ed FMLs are compared to CFRPs. In this analysis, the complete production, inspection and operational program has to be considered. If, after this analysis, the concept comes out as the best material choice, a more detailed testing program has to be started.

First part of this program is the study of the crack initiation. Although it is, based on theory, possible to claim that crack initiation does not occur in the FSW-ed sheets at the expected stress levels, a more thorough analysis is recommended. In this analysis, the reliability and feasibility of the weld inspection program has to be evaluated. The inspection method that finds defects larger than the maximum allowable defect size is ultrasonic phased array scanning. By inspecting FSW-ed samples for defects using this method and subsequently fatigue test them at the maximum expected stress range, it is possible to check the 'no crack-initiation'-theory. If crack initiation is not observed, it can be concluded that crack initiation will not occur for this specific combination of production, inspection and operational conditions. A benefit of this situation is that, if crack initiation is not observed in the welded region, it is possible to view FSW-ed FMLs as a standard material, which

implies that no joint-specific compliance requirements have to be met.

The second part of the detailed testing program would then consist of standard fatigue crack growth and residual strength tests on the new concept. If the measured crack growth rate and residual strength have moved to the desired levels, it can be concluded that the concept meets all of the set requirements. One test that was not performed in the current research, was the determination of the K_R-curve for Glare 3-3/2-0.4-FSW. This test would provide the information necessary to see if the new concept also meets the SSD residual strength requirements. If it cannot be shown that crack initiation will not occur, the complete DT certification plan has to be followed for a specific location in the aircraft structure. Note, however, that this can only be done after the adjusted crack growth and residual strength calculation methods have been validated.

After all of the checks, analyses, and tests have been completed, and successfully passed, the new method for joining FML panels is finally ready to be applied in aircraft structures. This research set the guidelines for application of FMLs with FSW-ed metal sheets in these structures and defined the limitations on the use of the material.

Bibliography

[1] Airbus, 2013. *Emirates Airline President Tim Clark: The A380 "defies gravity" in its success story.* [online] Available at: <http://www.airbus.com/newsevents/news-events-single/detail/emirates-airline-president-tim-clark-the-a380-defies-gravity-in-its-success-story/> [Accessed 9 Januari 2014].

[2] Airbus, 2013. *Airbus A380 technology.* [online] Available at: <http://www.airbus.com/aircraftfamilies/passengeraircraft/a380family/innovation/> [Accessed 9 Januari 2014].

[3] Vogelesang, L.B. and Vlot, A., 2000. Development of fibre metal laminates for advanced aerospace structures. *Jounal of Materials Processing Technology*, 103(1), pp.1-5.

[4] Vlot, A. and Gunnink, J., 2001. *Fiber Metal Laminates an introduction.* 2nd ed. Dordrecht: Kluwer Academic Publishers.

[5] Roebroeks,G., 1995. *The Development of the Splice Geometry for the Daimler-Benz Aerospace Airbus Glare 3-3/2-0.3 Barreltest Panel 1&2, Report TD-R-93-005B.* Delft: Stuctural Laminates Company.

[6] Vermeeren, C.A.J.R., Beumler, TH., De Kanter, J.L.C.G., van der Jagt, O.C. and Out, B.C.L., 2003. Glare Design Aspects and Philosophies *Aerospace Composite Materials*, 10(1), pp.257-276.

[7] Mishra, R.S. and Ma, Z.Y., 2005. Friction stir welding and processing *Materials Science and Engineering R: Reports*, 50(1-2), pp.1-78P.

[8] Speijer, J.L., 2009. *Ultrasonic C-scan inspection of Airbus A380 Glare fuselage panels.* [online] Fokker. Available at: <http://www.ndt.aero/formulieren/Presentation%20C-scan%20Glare%20-%20NANDT%2018-11-2009%20WEB-version.pdf> [Accessed 14 Januari 2014].

[9] Bied-Charreton, D., TBP. *Effects of defects in FSW in FMLs.* MSc. Delft University of Technology.

[10] Leonard, F., Shi, Y., Soutis, C., Withers, P.J. and Pinna, C., 2014. In: Fifth Conference on Industrial Computed Tomography, Upper Austrian University of Applied Sciences, Wels, 26 February, 2014, Austria.

[11] Pantelakis, S. and Rodopoulos, C., 209. *Engineering Agains Fracture* 1st ed. Houten: Springer Netherlands

[12] Threadgill, P.L., Leonard, A.J., Shercliff, H.R. and Withers, P.J., 2009. Friction stir welding of aluminium alloys. *International Materials Review*, 54(2), pp.49-93.

[13] Galvo, I., Leito, C., Loureiro, A. and Rodrigues, D., 2012. Friction Stir Welding of very thin plates. *Soldagem & Inspeo*, 17(1)

[14] Mahoney, M.W., Rhodes, C.G., Flintoff, J.G., Spurling, R.A. and Bingel, W.H., 1998. Properties of Friction-Stir- Welded 7075-T651 Aluminum. *Metallurgic and Materials Transactions A*, 29(1), pp.1955-1963.

[15] Biallas, G., Brain, R., Donne, C.D., Staniek, G. and Kaysser, W.A., 1999. In: Proceedings of the First International Symposium on Friction Stir Welding, Thousand Oaks, CA, 14-16 June, 1999, USA.

[16] Ilman, M.N., Kusmono and Iswanto, P.T., 2013. Fatigue crack growth rate behaviour of friction-stir aluminium alloy AA2024-T3 welds under transient thermal loading. *Materials and Design*, 50(1), pp.235-243.

[17] Ali, A., Brown, M.W. and Rodopoulos, C.A., 2008. Modeling of crack coalescence in 2024-T351 Al alloy friction stir welded joints. *International Journal of Fatigue*, 30(10-11), pp.2030-2043.

[18] Moreira, P.M.G.P. and Castro, de, P.M.S.T., 2012. Fatigue crack growth on FSW AA2024-T3 aluminum joints. *Key Engineering Materials*, 498(1), pp. 126-138.

[19] Lemmen, H.J.K., 2011. *Fatigue and Damage Tolerance of Friction Stir Welded Joints for Aerospace Applications*. PhD. Delft University of Technology.

[20] Arbechast, W.J., 2003. *Friction Stir Joining: Characteristic Defects*. Rapid City: Advanced Materials Processing Center.

[21] Mandache, C., Levesque, D., Dubourg, L. and Gougeon, P., 2012. Non-destructive detection of lack of penetration defects in friction stir welds. *Science and Technology of Welding and Joining*, 0(0), pp.1-9.

[22] Dickerson, T.L. and Pzydartek, J., 2002. Fatigue of friction stir welds in aluminum alloys that contain root flaws. *International Journal of Fatigue*, 25(1), pp.1399-1409.

[23] Zhou, C., Yang, X. and Luan, G., 2006. Effect of root flaws on the fatigue property of friction stir welds in 2024-T3 aluminum alloys. *Materials Science and Engineering*, 418(1), pp.155-160.

[24] Sato, Y.S., Takauchi, H., Park, S.H.C. and Kokawa, H., 2005. Characteristics of the kissing-bond in friction stir welded Al alloy 1050. *Materials Science and Engineering*, 405(1), pp.333-338.

[25] Federal Aviation Administration, 2011. *Advisory Circular 25.571-1D: Damage Tolerance and Fatigue Evaluation of Structure* [pdf] FAA. Available at: <http://www.faa.gov/documentLibrary/media/Advisory_Circular/AC%2025.571-1D%20.pdf> [Accessed 15 Januari 2014].

[26] European Aviation Safety Agency, 2013. *Certification Specifications and Acceptable Means of Compliance for Large Aeroplanes CS-25* [pdf] EASA. Available at: <http://www.easa.europa.eu/agency-measures/docs/agency-decisions/2013/2013-033-R/Annex%20to%20ED%20Decision%202013-033-R.pdf> [Accessed 28 Februari 2014].

[27] Homan, J.J., 2006. Fatigue initiation in fibre metal laminates. *International Journal of Fatigue*, 28(1), pp.366-374.

[28] Spronk, S.W.F, Sen, I. and Alderliesten, R.C., 2015. Predicting fatigue crack initiation in fibre metal laminates based on metal fatigue test data. *International Journal of Fatigue*, 70, pp.428-439.

[29] Alderliesten, R.C., 2007. Analytical prediction model for fatigue crack propagation and delamination growth in Glare. *International Journal of Fatigue*, 29(1), pp.628-646.

[30] Yang, J.M., Hahn, T.H., Seo, H., Chang, P.Y., and Yeh, P.C., 2010. *Damage Tolerance and Durability of Fiber-Metal Laminates for Aircraft Structures* [pdf] FAA. Available at: <http://www.tc.faa.gov/its/worldpac/techrpt/ar1018.pdf> [Accessed 21 October 2014].

[31] Khan, S.U., Alderliesten, R.C., Rans, C.D. and Bendictus, R., 2010. Application of a modified Wheeler model to predict fatigue crack growth in Fibre Metal Laminates under variable amplitude loading. *Engineering Fracture Mechanics*, 77(1), pp.1400-1416.

[32] Vries, de, T.J., 2001. *Blunt and sharp notch behaviour of Glare laminates*. Delft: Delft University Press.

[33] Mller, R.P.G., 1995. *An Experimental and Analytical Investigation on the Fatigue Behavior of Fuselage Riveted Lap Joints*. PhD. Delft University of Technology.

[34] ASTM Standard E561, 2004, *Standard Test Method fro K-R Curve Determination*, ASTM International, West Conshohocken, PA, 2003, DOIL 10.1520/E0561-10E02, www.astm.org

[35] Rijck, de, J.J.M., 2005. *Stress Analysis of Fatigue Cracks in Mechanically Fastened Joints*. PhD. Delft University of Technology.

[36] Wang, W., In progress. *Multiple Site Damage in Fibre Metal Laminates*. PhD. Delft University of Technology.

[37] Rans, C.D., Moriniere, F.D., Rodi, R., Alderliesten, R.C. and Benedictus, R., 2011. Fatigue behavior of fiber/metal laminate panels containing internal carbon tear straps. *Journal of Aircraft: devoted to aeronautical science and technology*, 48(6), pp.2122-2129.

[38] Jagt, van der, O.C., 2002. *Residual Strength of Damaged Glare Shells*. Delft: TU Delft.

[39] Vries, de, T.J. and Holleman, E., 1995. *An R-curve approach to fracture toughness analysis of some GLARE grades*. Delft: TU Delft.

[40] ASTM Standard E647, 2004, *Standard Test Method for Measurement of Fatigue Crack Growth Rates*, ASTM International, West Conshohocken, PA, 2003, DOI: 10.1520/E0561-10E02, <http://www.astm.org>

[41] AITM 1-0042, 2001, *Determination of Fatigue Crack Growth Rates for Aluminium Clad Sheet and Clad Plate up to 12 mm in Constant-Amplitude Tests - K-Increasing Method*, Airbus Industrie, Blagnac, France

[42] Shim, D.J., Alderliesten, R.C., Spearing, S.M. and Burianek, D.A., 2003. Fatigue crack growth prediction in GLARE hybrid laminates. *Composites Science and Technology*, 63(1), pp.1759-1767.

[43] Vlot, A., Vogelesang, L.B. and de Vries, T.J., 1999. Towards application of fibre metal laminates in large aircraft. *Aircraft Engineering and Aerospace Technology*, 71(6), pp.558-570.

[44] Takahasi, K., Muller, C., Ronneteg, U. and Pitkanen, J., 2009. *Probability of Detection from C-Scan Data for Reliability Analysis of Ultrasonic Non-Destructive Testing* [online] DGZIP. Available at: <http://www.ndt.net/article/reliability2009/Inhalt/th4b2.pdf> [Accessed 27 March 2014].

[45] Bisle, W., Meier, T., Mueller, S. and Rueckert, S., 2006. *In-Service Inspection Concept for GLARE - An Example for the Use of New UT Array Inpsection Systems* [online] ECNDT. Available at: <http://www.ndt.net/article/ecndt2006/doc/Tu.2.1.1.pdf> [Accessed 27 March 2014].

[46] Fokker. *Along the bondline*. [online] Fokker. Available at: <http://www.fokker.com/sites/default/files/media/Files/Brochures/Fokker_Glare.pdf> [Accessed 11 November 2014].

[47] Ratwani, M.M., 2000. *Inspection Technologies* [online] R-Tec. Available at: <http://ftp.rta.nato.int/publiC/PubFullText/RTO/EN/RTO-EN-015/EN-015-14.pdf> [Accessed 27 March 2014].

[48] Hatamleh, O., Lyons, J. and Forman, R., 2007. Laser and shot peening effects on fatigue crack growth in friction stir welded 7075-T7351 aluminum alloy joints. *International Journal of Fatigue*, 29(3), pp.421-434.

[49] Murman, E., Walton, M. and Rebentisch, E., 2000. Challenges in the Better, Faster, Cheaper Era of Aeronautical Design, Engineering and Manufacturing. *Aeronautical Journal*, 1040(104), pp.481-489.

[50] Tavares, S.M.O., 2011. *Design and Advanced Manufacturing of Aircraft Structures using Friction Stir Welding*. PhD. University of Porto.

[51] Kaufmann, M., Czumanski, T. and Zenkert, D., 2009. Manufacturing Process Adaptation for Integrated Cost/Weight Optimisation of Aircraft Structures. *Plastics, Rubber and Composites*, 38(2), pp.162-166.

[52] Mendez, P. and Eagar, T., 2002. New Trends in Welding in the Aeronautic Industry in: 2nd Conference New Manufacturing Trends for Aeronautical Industrie, Bilbao, 19-20 November, 2002, Spain.

[53] Ashby, M.F., 2005. *Materials Selection in Mechanical Design*. 3rd ed. Oxford: Elsevier Butterworth-Heinemann.

[54] Tipaji, P., 2007. *E-design Tools for Friction Stir Welding: Cost Estimation Tool*. Master's thesis. Missouri University of Science and Technology.

[55] Di Lorenzo, R. and Fratini, L., 2005. *A Cost Model for the Friction Stir Welding Process* In:Proceedings of EASFORM 2005, 8th international Conference of the European Scientific Association for Metal Forming, Cluj, 27-29 April, 2005, Romania.

[56] Laan, van der, A., Curran, R., Tooren, van, M. and Ritchie, C., 2006. Integration of Friction Stir Welding into a Multi-Disciplinary Aerospace Design Framework. *Aeronautical Journal*, 11(1), pp.759-766.

[57] Defalco, J., 2006. Friction Stir Welding vs. Fusion Welding. *Welding Journal*, 85(3), pp.42-44.

[58] ASM matweb, 2015. *Aluminum 2024-T3*. [online] Available at: <http://asm.matweb.com/search/SpecificMaterial.asp?bassnum=MA2024T3> [Accessed 12 Januari 2015].

[59] Dacko, A. and Toczynski, J., 2010. Structural response of a blast loaded fuselage. *Journal of KONES*, 17(1), pp.101-109.

[60] Aircraft Spruce, 2015. *2024T3 ALCLAD Aluminum*. [online] Available at: <http://www.aircraftspruce.com/catalog/mepages/alumsheet_2024t3.php> [Accessed 12 Januari 2015].

[61] Liu, Q., 2008. *An Effective Life Extension Technology for 7xxx Series Aluminium Alloys by Laser Shock Peening* [pdf] Australian Government Department of Defence. Available at: <http://dspace.dsto.defence.gov.au/dspace/handle/1947/9655> [Accessed 12 Januari 2015].

Appendices

A

Details experimental results

Since not every step for the experimental part of this research was covered in full detail in the main part of this report, this appendix gives a more detailed view of all the reasoning involved in arriving at the results from chapter 5. Just like this chapter, the appendix is split in the subsections SSD crack initiation and growth, MSD crack initiation and growth, and MSD residual strength.

A.1 SSD crack initiation and growth

In the section on SSD crack initiation and growth, two areas can be found that require a more detailed look than that provided in the main report: the conversion of the measured crack growth rate to the effective crack growth rate and the determination of the collipriest parameters for the analytical model.

From measured crack growth rate to effective crack growth rate

In the SSD crack initiation and growth section the conversion of measured crack growth rate to effective crack growth rate is mentioned. Everything about this conversion is already covered in the main body of the report, except for the quantification of the difference between these two growth rates. For illustration purposes, the difference between the measured crack growth rate (considering only the FSW-ed layer) and the effective crack growth rate is indicated in figure A.1.

Determining the collipriest parameters for the analytic calculations

The set of collipriest parameters (C1=-3.667, C2=1.90, m=0.42) used to predict the effective crack growth rate as a function of the SIF was iteratively determined from the crack growth data obtained from the experiments. By adjusting the variables C1 (which determines the crack growth rate at K_{tip}=0) and C2 (the increase in crack growth rate for an increase in SIF) it was possible to fit the model to the experimental data. The final set of variables provided a decent fit for the measured crack growth; the average crack growth rate as a function of the crack size was closely met, but the detailed increase in crack growth rate for an increase in crack size could not be modeled.

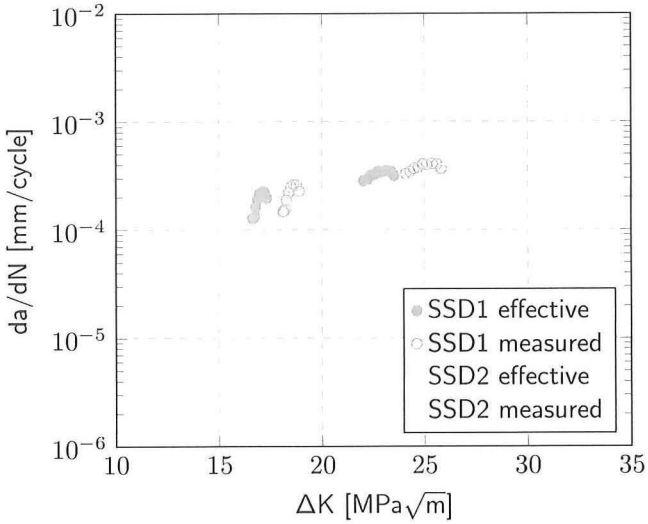

Figure A.1: Measured crack growth resistance vs. the effective crack growth resistance.

Despite this mismatch, the model still shows a lot of potential for both the effective crack length as well as the real crack length. In order for this model to work for the real crack length it is necessary to determine the crack size in each layer separately and calculate the force redistribution (based on the change in Young's moduli) over the layers after each cycle. This also implies that the residual welding stresses and the crack growth rate parameters for the FSW-ed layer need to be known. If all of this is implemented in this model, it is to be expected that the real crack growth rate can be modeled using the current method.

A.2 MSD crack initiation and growth

In the section on MSD crack initiation and growth the only points that requires a more detailed look are the crack morphology of the MSD test specimens and the derivation of the outer layer crack growth- to center layer crack growth- conversion.

Crack morphology MSD test specimens

One of the most notable observations from the MSD crack growth tests was that cracks initiated at the retreating side of the weld at locations where weld flash was visible. Whereas, in MSD7, this happened after the cracks initiated from the notches and linked-up, in MSD5 cracks only formed at the weld flash directly located under the notches. Figure A.2 shows the weld flash cracks visible in MSD7. As can be seen from the figures the cracks formed at the left and right side of the specimen and in between notch 1 and 2, as seen from the left side.

Since these kind of cracks only formed in the MSD specimens with the FSW-ed layer as the outer layer it is expected that the cracks formed due to local stress concentrations and can therefore be avoided by removing the weld flash before lay-up.

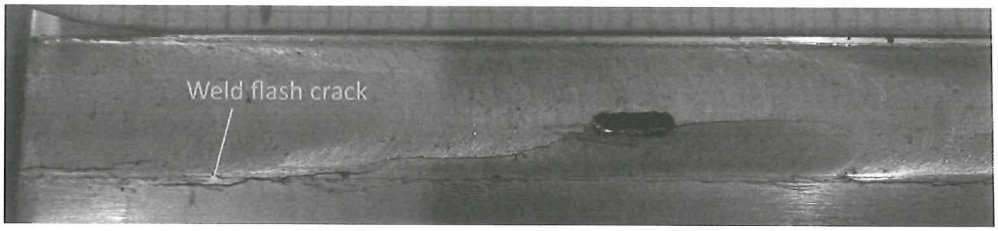

(a) Left section

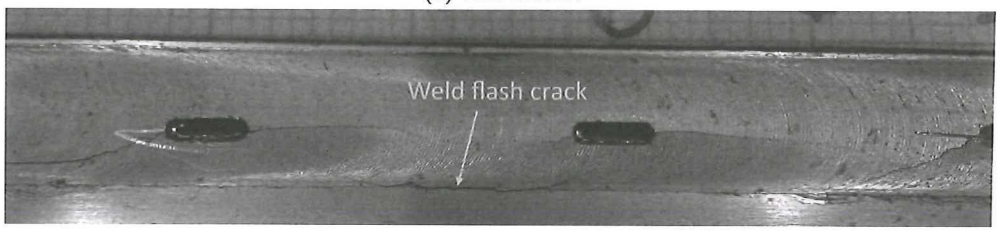

(b) Center section

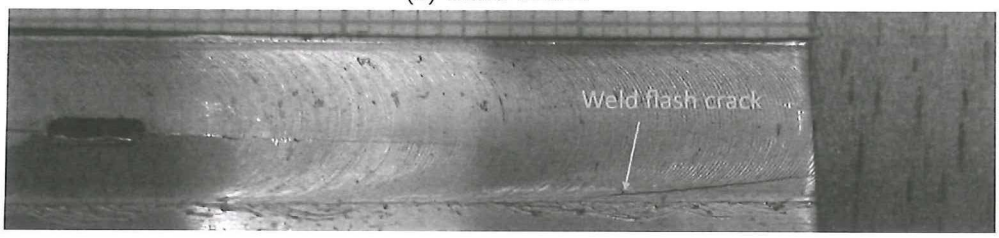

(c) Right section

Figure A.2: Weld flash cracks at the retreating side in MSD7.

Outer layer crack growth- to center layer crack growth- conversion

As was already explained in the concerning section, the crack growth conversion is based on the proportion of crack growth visible in the FSW-ed sheet of the MSD4 specimen after 120,000 cycles and the crack growth in the FSW-ed sheet of the MSD8 specimen after the same amount of cycles. By multiplying the crack growth rate in the FSW-ed sheet of MSD8 by the conversion factor it is possible to predict the crack growth rate in the welded sheet of MSD4.

An example of this prediction would be the results from figure A.3. This figure shows the crack growth rate as a function of the crack length for MSD4,7 and 8. The crack growth rates for MSD7 and MSD8 are measured values, whereas the crack growth rate in the MSD4 specimen is assumed to be 0.476 times the crack growth rate in the FSW-ed sheet of the MSD8 specimen. Instead of using this as a prediction for the crack growth rate in specimens with the FSW-ed sheet as the center layer, the real crack growth rate (for specimens that have slits only in the center layer) would be 0.476 times the measured crack growth rate in the MSD7 specimen of which the results are shown in the main report.

A.3 MSD residual strength

In addition to the explanation of the stress-strain behavior of the different MSD specimens already given in the main part of the report, this appendix provides a more illustrative example.

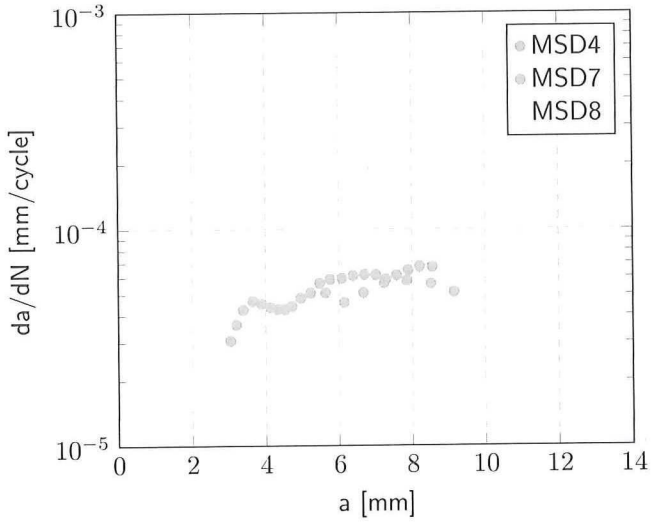

Figure A.3: Average crack growth rate in the FSW-ed sheet vs. the crack length for MSD specimens.

As has been noted before, the stress-strain curves of the specimens with cracks only in the outer layer differ from the curves of the specimens with cracks in multiple layers. This behavior is depicted in figure A.4, which shows the stress-strain curves for MSD1 and MSD7.

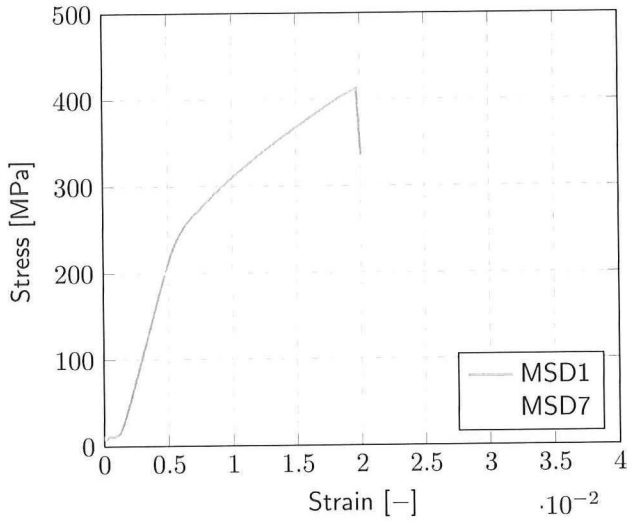

Figure A.4: Stress-strain curves showing the typical behavior of the different specimens.

From the figure it can be seen that the curve for MSD1 (one of the specimens with slits going trough two metal layers) has an initial linear elastic part, followed by plastic deformation and abrupt failure. Whereas this can be qualified as typical stress-strain behavior for standard Glare, MSD7 (one of the specimens with slits in the outer layer only) shows different behavior. The main difference between

the two is the failure of the FSW-ed layer in MSD7 far before the rest of the laminate fails. This failure is clearly visible in the curve at a strain of around 0.004.

B

Value analysis of the conceptual designs

In addition to the information already presented in section 6.3, this appendix provides a more detailed view on the calculations and reasoning involved in the process of selecting the best concept. The first section of this appendix considers the derivation of the equation for the DOC per unit length, and the second, and last, section the calculations on the value of the different concepts.

B.1 Derivation of the direct operating cost

The direct operating cost per unit length is, as was already mentioned in the chapter on value analysis, the sum of the manufacturing cost and the operating cost:

$$DOC = C_{man} + pM_s \tag{B.1}$$

Since the main goal of the analysis is to create a ranking of the design concepts, it is possible to subtract the costs all of the concepts have in common. For this specific case, this would be the cost of a Glare 3 panel per unit length:

$$\Delta DOC = DOC_{concept} - DOC_{Glare3} \tag{B.2}$$

The new DOC can therefore be written as:

$$\Delta DOC = \Delta C_{man} + p\Delta M_s \tag{B.3}$$

In this equation p is a life-time fuel cost factor with a value of 161.8 €/kg [52], ΔM_s the increase in mass of the structure compared to standard Glare per unit length, and ΔC_{man} the increase in manufacturing cost per unit length compared to standard Glare. The increase in mass of the structure is given by:

$$\Delta M_s = \rho_{al}\Delta A_{al} + \rho_{pre}\Delta A_{pre} + \rho_{extra,1}\Delta A_{extra,1} + ... + \rho_{extra,n}\Delta A_{extra,n} \tag{B.4}$$

Here ρ is the density of the material, ΔA the increase in cross-sectional area of the material, and the subscripts al, pre, and $extra$, aluminum, prepreg and extra materials respectively. The increase in manufacturing cost per unit length is given by:

$$\Delta C_{man} = \Delta C_{prod} + c_{al}\Delta A_{al} + c_{pre}\Delta A_{pre} + c_{extra,1}\Delta A_{extra,1} + ... + c_{extra,n}\Delta A_{extra,n} \tag{B.5}$$

Where c is the cost of the material per unit volume and ΔC_{prod} the increase in production costs per unit length compared to standard Glare. This last variable covers equipment, labour, energy and costs for consumables.

Although there are methods that consider all these costs separately, such as [54, 55, 56] for FSW-ing for example, it is hard to determine the individual components. Therefore it was decided to use the method as presented by Tavares and Defalco [50, 57], in which all of the components are combined into one number.

B.2 Calculations on the value of the different concepts

The values for the constants used in the analysis are presented in table B.1. Two of the values shown in this table require a closer look. First, is the value for the density of the fill material (the pink material in the figures of the concepts). In the analysis it was assumed that the density of this material was equal to the density of the prepreg. Due to the relatively small amount compared to the other materials, this is considered to be an assumption that does not influence the final ranking of the concepts.

Second, is the production cost of laser peening. As can be seen from the table, the costs of this process are significantly higher than that of FSW-ing alone. The only source that provided information on the cost of this process was [61]. Since the costs of laser peening may have decreased since that time, the calculated value for concept 4 should be seen as a conservative estimation. This value was calculated based on the assumption that both sides of the welds were peened over a width of 14 mm.

Table B.1: Values for the constants used in the analysis.

p [€/kg]	ρ_{al} [kg/mm^3]	ρ_{pre} [kg/mm^3]	ρ_{fill} [kg/mm^3]	c_{al} [€/mm^3]	$C_{prod,FSW}$ [€/mm]	$C_{prod,laser}$ [€/mm]
161.8 [52]	2.78E-6 [58]	8.91E-7 [59]	8.91E-7 [59]	7.1E-3 [60]	2.5E-3 [50]	4.58 [61]

Next to the value of the constants, the only things that were needed to determine the value of the concepts were the change in cross-sectional area of the different materials and the change in production costs compared to the standard laminate. The final values for these variables are shown in table B.2.

Table B.2: Change in cross-sectional area and production costs, compared to standard Glare.

Concept	ΔA_{al} [mm^2]	ΔA_{pre} [mm^2]	ΔA_{fill} [mm^2]	ΔC_{prod} [€/mm]
Splice	3.04	0.00	2.00	0.00
FSW-ed Glare	0.00	0.00	0.00	0.0075
Concept 1	69.20	0.00	0.80	0.0075
Concept 2	0.00	84.59	0.80	0.0075
Concept 3	51.90	38.57	0.87	0.0075
Concept 4	0.00	0.00	0.00	27.48

The values for the production costs in this table only show the costs of processes such as FSW-ing and laser peening. Since no good estimate for the lay-up time could be given, lay-up labour costs were not considered in the ranking of the 4 concepts.

Although the differences in lay-up time between the 4 concepts will be small, a bigger difference was to be expected between the selected concept (concept 1) and the spliced version of the laminate. To make these two concepts comparable it was assumed that it takes 3 minutes of extra work (at an hourly rate of 60 €/hr), compared to the standard laminate, to lay-up a 1000 mm long concept 1 joint. The fraction of extra work involved in laying up a splice of the same length (defined as the labour rate) was calculated and plotted against the value of the splice joint in figure B.1.

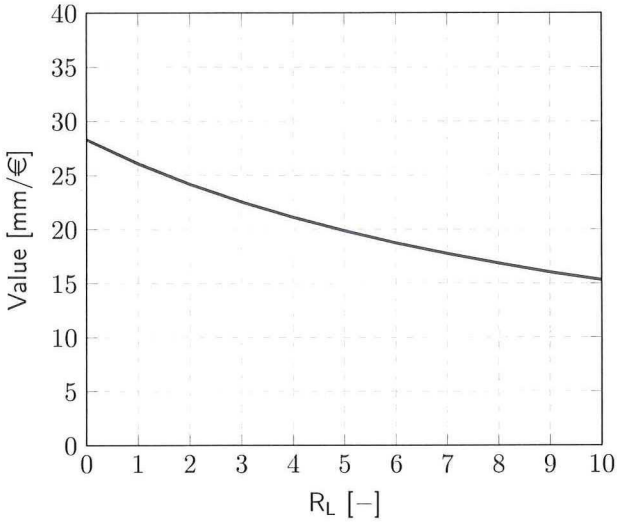

Figure B.1: Value for the spliced version of the laminate vs. the labour rate.

As can be seen from this figure, the value of the splice joint remains bigger than the value of concept 1, even if it takes 10 times longer to lay-up the splice joint.

Samenvatting

Vermoeidheid en Schade Tolerantie van Wrijvingsroerlassen in Vezel Metaal Laminaten

Derk Doppenberg

Splicing is een methode om Vezel Metaal Laminaat (VML) panelen te verbinden door, op de locatie van de verbinding, de metalen lagen te laten overlappen om zo een Schade Tolerante (ST) binding te vormen. Deze verbindingsmethode wordt succesvol toegepast in vliegtuigconstructies, maar heeft één groot nadeel; het kan niet gebruikt worden in constructies met een significante dubbele kromming. Om VML-en ook voor deze locaties geschikt te maken, is een andere verbindingsmethode nodig. Met dit in gedachten werd het idee van gewrijvingsroerlaste VML-en geboren. Door de metalen lagen aan elkaar te wrijvingsroerlasssen voor het opleggen, wordt het mogelijk om VML constructies te maken met de vereiste dubbele kromming. Dit onderzoek is erop gericht om de ST ontwerpprincipes te ontwikkelen voor een succesvolle toepassing van dit concept in vliegtuigconstructies.

Om dit doel te bereiken, werd een stap-voor-stap ST aanvaardingsplan opgesteld. Dit plan begon met het identificeren van analytische methodes die gebruikt kunnen worden om de ST prestaties van de verbinding te voorspellen. In de daaropvolgende stappen werden relaties tussen de ST eigenschappen van gewrijvingsroerlaste Glare 3-3/2-0.4 en standaard Glare 3-3/2-0.4 experimenteel bepaald, en gebruikt om verschillende concepten te ontwerpen die voldeden aan de eisen van het aanvaardingsplan. Uit deze vier concepten werd het idee met de hoogste waarde met betrekking tot de kosteneffectiviteit gekozen, en vergeleken met andere materialen die veel gebruikt worden in de luchtvaartindustrie.

Experimentele resultaten lieten zien dat scheuren sneller groeiden in- en reststerkte lager was van de gewrijvingsroerlaste versie van het laminaat. Om de ST prestaties terug te brengen naar het niveau van het standaard laminaat, zijn extra lagen materiaal nodig ter plaatse van de lassen. Het concept dat dit op de meest kosteneffectieve manier doet voor Glare 3-3/2-0.4, is een verbinding met een inter-laminaire aluminium dubbeler van dezelfde dikte als de andere aluminium lagen. Vergeleken met de splice-versie van het laminaat, is het gewrijvingsroerlaste concept significant duurder. Als men kijkt naar de ST prestaties ten opzichte van andere materialen, presteren alleen sommige koolstofvezel versterkte plastics beter.